Passive Acoustic Detection and Measurement of Rainfall at Sea

BARRY B. MA AND JEFFREY A. NYSTUEN

Applied Physics Laboratory, University of Washington, Seattle, Washington

(Manuscript received 4 November 2003, in final form 31 July 2004)

ABSTRACT

Rainfall over the ocean is one of the most important climatic parameters for both oceanic and atmospheric science. Traditional accumulation-type rain gauges are difficult to operate at sea, and so an alternate technique using underwater sound has been developed. The technique of passive monitoring of the ocean rainfall using ambient sound depends on the accuracy of sound pressure level (SPL) detection. Consequently, absolute calibration of the hydrophone is desirable, but is difficult to achieve because typically the geometry of the laboratory calibration process does not fit the measurement geometry over the ocean. However, if one assumes that the sound signal that is generated by wind is universal then the wind signal can be used to provide an absolute calibration. Over 90 buoy months of ambient sound spectra have been collected on the Tropical Atmosphere Ocean (TAO) project array since 1998. By applying the Vagle et al. wind speed algorithm, the instrument noises and sensitivity bias for the absolute calibration of each acoustic rain gauge (ARG) are obtained. An acoustic discrimination process is developed to retrieve the pure geophysical signals. A new single-frequency rainfall-rate algorithm is proposed after comparing the ARG data with R.M. Young self-siphoning rain gauge data, collocated on the same moorings. The acoustic discrimination process and the rainfall algorithm are further tested at two other locations and are compared with R.M. Young rain gauges and the Tropical Rain Measuring Mission (TRMM) product 3B42. The acoustic rainfall accumulations show the comparable results in both long (year) and short (hours) time scales.

1. Introduction

The ocean ambient noise has long been noted as presenting an "unwanted" background sound at any given location and time. Different sources of ambient sound contribute to the overall sound level at different frequency ranges and time spans. Some of the sources are also heavily dependent on the location. For example, at some continental shelf regions, biological sounds related to a particular fish could be the dominant ambient noise source. Sites near ocean shipping lanes are much noisier than other open-ocean locations at the low frequencies. For the higher frequencies (50 kHz plus) thermal noise is a dominant source, whereas the other sources are often attenuated. For the frequency range from 1 to 50 kHz, wind-generated noise is the major persistent noise source component, characterized by a spectrum with a uniform negative slope. However, when rain is present, the rain-generated sound usually dominates all of the other sources in this frequency band. In summary, the ocean ambient sound is time, frequency, and location dependent. If one can detect when a particular dominant source is present (e.g., rain), then that "unwanted noise" can be treated as a "wanted signal," and can be used to quantify its presence. The temporal and frequency distribution of typical sources of ocean ambient sound are illustrated in Fig. 1.

Rainfall measurement over the ocean is very difficult to achieve because of its inhomogeneity in both time and space. Furthermore, the natural roughness of the air–sea interface produces a potentially catastrophic environment for surface instruments on moorings, and this is reflected in the data quality from physical collection types of rain gauges on moorings. Other techniques for measuring the rainfall over the ocean use satellite-based instruments. These should provide a

Corresponding author address: Dr. Barry Ma, Applied Physics Laboratory, University of Washington, Box 355640, 1013 NE 40th St., Seattle, WA 98105-6698.
E-mail: binbing@u.washington.edu

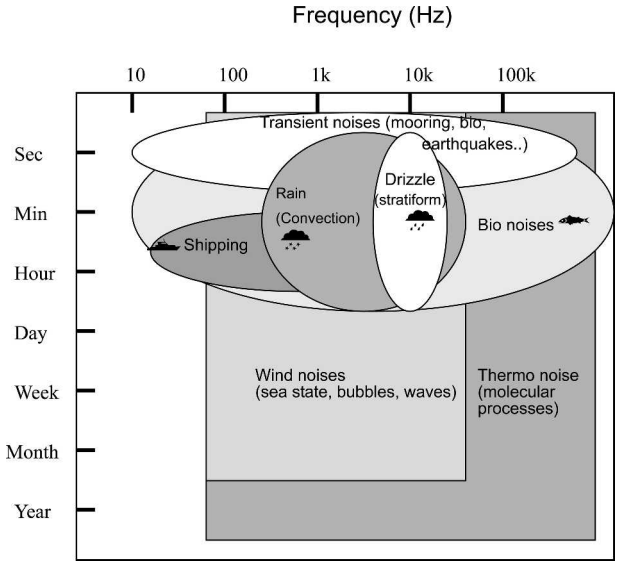

FIG. 1. The temporal and frequency distribution of typical sources of ocean ambient sound.

large-scale coverage for the measuring of different parameters associated with rainfall. However, the satellite's temporal resolution is usually very low (e.g., eight satellite passes per day). In addition, surface truth measurements are needed for rainfall. Luckily, rain is also one of the principal natural sources of underwater sound (Nystuen et al. 2000). This allows for acoustic measurements of rainfall. Although there are sometimes man-made or biological noises that are loud and could potentially interfere with the acoustical measurement of rain, these noises are generally intermittent or geographically localized.

This paper first describes some background information and other ancillary data used in this study. A new method is proposed using the Vagle et al. (1990) wind speed algorithm to determine the frequency-dependent instrument noise and sensitivity bias to achieve the hydrophones' absolute calibration. The acoustic discrimination process for the qualification of pure geophysical signals is described. For quantification, an analytical approach is adopted by applying an orthogonal least squares regression between the acoustic rain gauge (ARG) data and a subset of 1-min-interval R.M. Young self-siphoning rain gauge data during the rainfall events to produce an empirical algorithm. The acoustic discrimination process and rainfall algorithm are further tested on the acoustic data from other deployments (10°N, 95°W and 12°N, 95°W), and are compared with the Tropical Rainfall Measuring Mission (TRMM) product 3B42 and R.M. Young rain gauges. The summary acoustic spectra for rainfall and the wind speed dependence on this acoustic rainfall signal are described at the end.

2. Background

Naturally occurring raindrops range in size from about a 300-μm diameter (a drizzle droplet) to over a 5-mm diameter (often at the beginning of a heavy downpour). As the drop size changes, the shape of the splash changes, and so does the subsequent sound production. Laboratory and field studies (Medwin et al. 1992; Nystuen 1996, 2001) had been used to identify five acoustic raindrop sizes (Table 1). For tiny drops (diameter < 0.8 mm), the splash is gentle, and no sound is detected. On the other hand, small raindrops (0.8–1.2-mm diameter) are remarkably loud. The impact component of their splash is quiet, but the geometry of the splash is such that a bubble is generated by every splash in a very predictable manner (Pumphrey et al. 1989). These bubbles are relatively uniform in size, as, therefore, is their frequency, and they are very loud underwater. Small raindrops are present in almost all types of rainfall, including light drizzle, and are, therefore, responsible for the remarkably loud and unique underwater "sound of drizzle" heard between 13 and 25 kHz—the resonance frequency for these bubbles. Interestingly, the splash of the next larger raindrop size—medium (1.2–2.0-mm diameter)—does not trap bubbles underwater; and, consequently, medium raindrops are relatively quiet, much quieter than the small raindrops. The only acoustic signal from these drops is a weak

TABLE 1. Acoustic raindrop sizes. The raindrop sizes are identified by different physical mechanisms associated with the drop splashes (Nystuen 2001).

Drop size	Diameter (mm)	Sound	Frequency range (kHz)	Splash character
Tiny	<0.8	Silent		Gentle
Small	0.8–1.2	Loud bubble	13–25	Gentle with bubble every splash
Medium	1.2–2.0	Weak impact	1–30	Gentle, no bubbles
Large	2.0–3.5	Impact, loud bubbles	1–35, 2–35	Turbulent; irregular bubble entrainment
Very large	>3.5	Loud impact, loud bubbles	1–50, 1–50	Turbulent, irregular bubble entrainment, penetrating jet

impact sound that is spread over a wide frequency band. For large (2.0–3.5-mm diameter) and very large (> 3.5 mm) raindrops, the splash becomes energetic enough that a wide range of bubble sizes are trapped underwater during the splash, producing a loud sound that includes relatively low frequencies (1–10 kHz) from the larger bubbles. For very large raindrops, the splat of the impact is also very loud, with the sound spread over a wide-frequency range (1–50 kHz). Thus, each drop size produces sound underwater with unique spectral features that can be used to acoustically identify the present of that drop size within the rain.

At any given time, the local hydrophone pressure at the measurement site can be expressed as the sum of all sound sources around the hydrophone in micropascals,

$$P_a = P_r + P_w + P_{\rm ss} + P_{\rm ml} + P_{\rm st} + P_{\rm other}, \qquad (1)$$

where *r, w,* ss, ml, and st denote rain, wind, sea state, marine life, and ship traffic, respectively (Black et al. 1997). The sound pressure level (SPL) in decibels can be expressed as

$$\mathrm{SPL}(f) = 10\log_{10}\left(\frac{P_a^2}{P_{\rm ref}^2}\right) \text{ dB relative to } 1\mu\mathrm{Pa}^2\mathrm{Hz}^{-1}, \qquad (2)$$

where P_a^2 is the variance of the pressure fluctuations in the 1-Hz bandwidth, and $P_{\rm ref}$ is the reference level at 1 μPa^2 Hz^{-1}. The contribution to the pressure fluctuation from different sources cannot be separated because they are indistinguishable. But, if different sources have a unique frequency spectrum SPL*(f)*, then times with only particular sources present can be identified, for example, P_w (wind only), P_r (rain only), and $P_r + P_w$ (rain and wind combined).

The pressure signal resulting from wind and rain comes from the ocean surface. If the sound source is assumed to be uniformly distributed, then the sound intensity at the source depth h below the surface can be related to the sound intensity at the surface I_0 by

$$I(h) = \int I_0 \cos^2\theta \,\mathrm{atten}(p)\, dA, \qquad (3)$$

where θ is the zenith angle and atten(p) describes the attenuation resulting from geometric spreading and absorption along the acoustic path p. By relating I_0 to rainfall rate, acoustic measurements at the rainfall rate can be obtained (Nystuen 2001). If absorption and refraction are neglected, the measurement should be independent of depth. For any particular deployment, the attenuation along the acoustic path can be complicated, but have only resulted in minor corrections in other studies (Vagle et al. 1990).

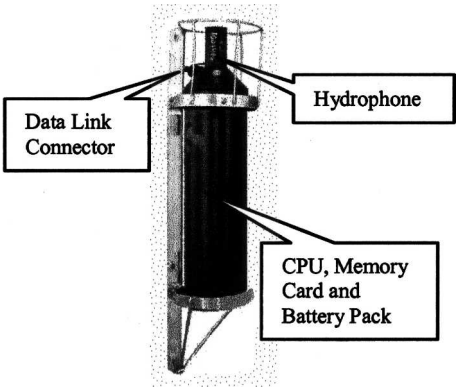

FIG. 2. Acoustic rain gauge.

3. The instrument—Acoustic rain gauges

The ARGs consist of an ITC-8263 hydrophone, signal preamplifiers, and a recording computer (Tattle-

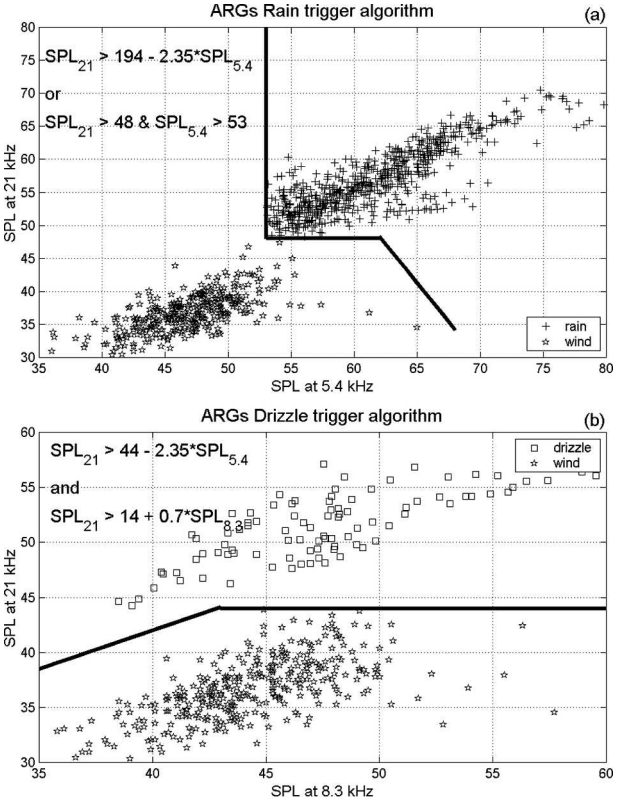

FIG. 3. The scatter diagram of (top) rain detection and (bottom) drizzle detection, which are the examples from ARG K that was deployed at 0°, 165°E in 2000. These algorithms are used for the initial screening of potential precipitation event and trigging the datalogging sequence on the ARGs.

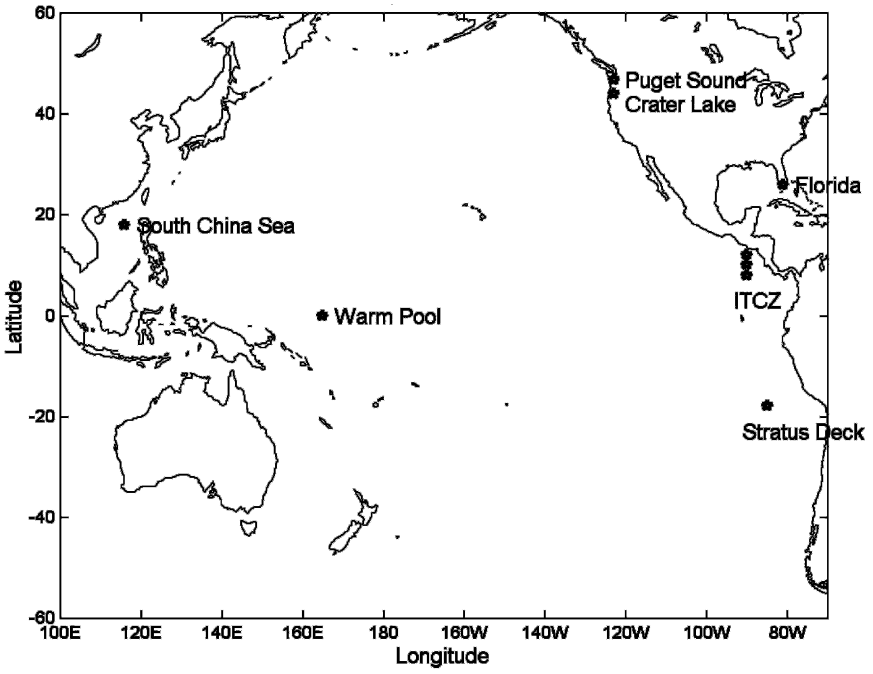

FIG. 4. The deployment of ARGs in different climate regions since 1996. The data at the Pacific warm pool and ITCZ, which have about a 90–buoy month acoustic record, are used in this study.

tale-8) (Fig. 2). The nominal sensitivity of these instruments is −160 dB relative to 1 V μPa^{-1}, and the equivalent oceanic background noise level of the preamplifier system is about 28 dB relative to 1 μPa^2 Hz^{-1}. Bandpass filters are present to reduce saturation from low-frequency sound (high pass at 300 Hz) and aliasing from above 50 kHz (low pass at 40 kHz). The ITC-8263 hydrophone sensitivity also rolls off above its resonance frequency at about 40 kHz. A data collection sequence consists of four 1024-point time series collected at 100 kHz (10.24 ms each), separated by 5 s if triggered by rain or drizzle. Each time series is fast Fourier transformed (FFT) to obtain a 512-point (0–50 kHz) power spectrum. These four spectra are averaged together and spectrally compressed to 64 frequency bins, with the frequency resolution of 200 Hz from 100 to 3000 Hz, and 1 kHz from 3 to 50 kHz. These spectra are evaluated individually to detect the acoustic signature of rainfall and then are recorded internally. Two algorithms are used for initial rainfall classification.

The rain-detection algorithm is

$$\mathrm{SPL}_{21\mathrm{kHz}} > 194 - 2.35\mathrm{SPL}_{5.4\mathrm{kHz}},$$

or

$$\mathrm{SPL}_{21\mathrm{kHz}} > 48\ \mathrm{dB} \quad \text{and} \quad \mathrm{SPL}_{5.4\mathrm{kHz}} > 53\ \mathrm{dB}. \tag{4}$$

The drizzle-detection algorithm is

$$\mathrm{SPL}_{21\mathrm{kHz}} > 44 \quad \text{and} \quad \mathrm{SPL}_{21\mathrm{kHz}} > 14 + 0.7\mathrm{SPL}_{8.3\mathrm{kHz}}. \tag{5}$$

These detection algorithms, Eqs. (4) and (5) for rain and drizzle, respectively, are designed to detect all possible rainfall situations. However, loud noises are also detected. This noise component of the data needs to be removed by a further classification analysis. The partition of detection algorithms is shown in Fig. 3.

The ARGs have been deployed on the Tropical Atmosphere Ocean project (TAO) moorings since 1998 at different locations with depths from 28 to 98 m. The depth was chosen to be above the thermocline to lessen the effects of acoustic refraction and maximize the sampling area, so that the buoy itself does not occupy a significant portion of the effective listening area. Equation (3) can be used to estimate the effective sampling area at the surface. Neglecting refraction and absorption, 90% of the signal arrives from a sampling area equal to

$$\text{Surface sampling area} \cong \pi(3h)^2, \tag{6}$$

where h is the depth of the hydrophone. The integrating area of the hydrophone is important for two reasons. First, rainfall is inhomogeneous on all scales, but

TABLE 2. The acoustic datasets used in this study: The asterisk (*) indicates the dataset used to produce the rainfall-rate algorithm. Note that the B and K ARGs are deployed in the same mooring but at different depths. The ARG settings for the difference condition are R: rain trigger, D: drizzle trigger, and W: wind only. [ARG A and B record 36 frequency channels with one spectrum for rain, drizzle, and wind in every sampling interval. The other ARGs record 64 frequency channels with four spectra for rain and drizzle (each separated by 5 s), and one spectrum for wind.]

	Deployment					
Location	ARG*	Log	Depth (m)	Record setting	Deploy period	Note
0°, 165°E	*, B	4	20	R-1 min D-4 min W-9 min	1 Mar 2000–20 Jul 2000	The wind estimate higher than R.M. Young anemometer by 0–2 m s^{-1}
0°, 165°E	*, K	1	50	R-1 min D-3 min W-9 min	1 Mar 2000–20 Jul 2000	Wind speed conversion well matched with R.M. Young anemometer
0°, 165°E	A	4	8	R-0.5 min D-4 min W-9 min	23 Jul 2000–20 Nov 2000	Noisy sample
0°, 165°E	*, D	1	98	R-1 min D-3 min W-9 min	23 Jul 2000–20 Nov 2000	Successful
0°, 165°E	A	5	28	R-0.5 min D-4 min W-9 min	Jul 2001–Jan 2002	Successful
0°, 165°E	G	2	98	R-1 min D-3 min W-9 min	Jul 2001–Nov 2001	Hydrophone malfunction after Nov
8°N, 95°W	G	1	38	R-1 min D-3 min W-9 min	Dec 1999–Mar 2000	Not much precipitation in this period
8°N, 95°W	L	1	38	R-1 min D-3 min W-9 min	22 Apr 2000–10 Nov 2000	Successful
10°N, 95°W	E	1	38	R-1 min D-3 min W-9 min	Dec 1999–Apr 2000	Not much precipitation in this period
10°N, 95°W	I	1	38	R-1 min D-3 min W-8 min	21 Apr 2000–Nov 2000	Strong local noise
10°N, 95°W	*, C	1	38	R-1 min D-3 min W-8 min	10 Nov 2000–16 Apr 2001	Acoustic data at first 100 day, then noise present in two 10–20-day periods
10°N, 95°W	L	2	38	R-1 min D-3 min W-9 min	Apr 2001–31 Mar 2002	Successful
12°N, 95°W	F	1	38	R-1 min D-3 min W-9 min	Dec 1999–Apr 2000	Not much precipitation in this period
12°N, 95°W	H	1	38	R-1 min D-3 min W-8 min	23 Apr 2000–2 Dec 2000	Periodical local noises present
12°N, 95°W	D	2	38	R-1 min D-3 min W-9 min	27 Mar 2001–1 Apr 2002	Successful

rainfall measurements are needed on large temporal or spatial scales. An instrument with a large inherent sampling area should produce a better "mean" rainfall statistic. Second, the large spatial sampling allows the short temporal sampling periods being used for each data sample to include many individual raindrop splashes (Nystuen 2001).

The temporal sampling strategy is designed to allow the instrument to record data for up to 1 yr and yet detect the relatively short time intervals associated with rainfall. To achieve this goal, the ARG enters a low-power "sleep mode" between each data sample. For these deployments, the ARGs "sleep" for 8–9 min and then sample the sound field. If "rain" is detected, the sampling rate changes to 1 min (or 3–4 min if "drizzle" is detected) and stays at the higher sampling rate until rain is no longer detected. For the rain- or drizzle-detected condition, four spectra are stored (separated by 5 s). For no-rain conditions, one averaged spectrum is stored.

The signal contains sound from the desired geophysical quantity, plus sounds from wind and noises from other sources. Two climate regions, the Pacific warm pool and intertropical convergence zone (ITCZ), have been chosen for this study. These open-ocean locations have less contribution from bottom reverberation and biological sources than from the continental shelf regions. About 90 buoy months of acoustic data are available for our analysis. ARGs have also been deployed in several different climate regions, as shown in Fig. 4. The acoustic datasets used in this study are listed in Table 2.

4. Ancillary data from the mooring and satellite

Pacific Marine Environmental Laboratory (PMEL) moorings data and TRMM satellite data are used in the intercomparison of ARG data for algorithm development and validation.

a. Data from ATLAS mooring

The next-generation Autonomous Temperature Line Acquisition System (ATLAS) buoys (Milburn et al.

1996; McPhaden et al. 1998) are deployed throughout the tropical Pacific and Atlantic Oceans. The ARGs were mounted on the mooring lines at the various locations. Selected ancillary datasets from the moorings are used in our study.

1) R.M. YOUNG ANEMOMETER DATA

The R.M. Young Company anemometer is mounted on the ATLAS mooring at a 4-m height. The data values are 10-min-averaged wind vectors. The error estimate is ± 0.3 m s^{-1} or 3% of the wind speed, whichever is greater (Freitag et al. 2001). By using the Tropical Ocean Global Atmosphere Coupled Ocean–Atmosphere Response Experiment (TOGA COARE) V2.5 flux algorithm (Fairall et al. 1996), these values are converted to an equivalent 10-m height wind speed. The 10-m winds are slightly stronger than 4-m wind values by factors of 1.010–~1.0217 in the calculation, which is smaller than the error estimate of the R.M. Young anemometer. The surface anemometer wind speed data are used to predict the ambient sound level at 8 kHz. This allows the sensitivity bias and instrument noise of the hydrophone to be identified.

2) R.M. YOUNG RAIN GAUGE DATA

Precipitation measurements on ATLAS buoys are made using R.M. Young Company model 50203-34 self-siphoning rain gauges mounted 3.5 m above the ocean surface. The instruments have a 100 cm^2 (11.3-cm diameter) catchment cylinder mounted on top of a fill tube. The measuring tube has a maximum capacity of 500 mL, which is equivalent to 50 mm of rainfall accumulation, after which it automatically drains via a siphon. Siphon events take about 30 s, and are typically identified by sharp declines in volume for two consecutive samples. In real-time processing, these events are ignored. The 1-min volume samples are stored on board the mooring while at sea, and are available for postprocessing after recovery. In postdeployment processing, data that are associated with siphon events are flagged, typically removing 3 min worth of data centered on the event. Once the mooring is recovered, the

TABLE 3. The measured sound pressure level (dB relative to 1 μPa^2 Hz^{-1}) vs corrected value, which uses 27.5 dB as background noise reference.

Measured SPL (dB)	Corrected SPL (dB)	Difference (dB)
30	26.41	3.59
40	39.74	0.26
50	49.97	0.03

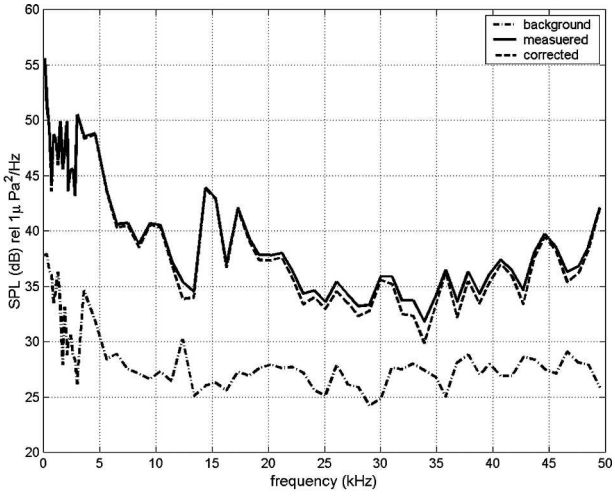

FIG. 5. The example of background noise removal. The dashed–dotted line is the background noise, which is the lowest spectrum from a weeklong record. The solid line is an arbitrary sample spectrum, and the dashed line is the corrected spectrum, which applied Eq. (10) to remove the background noise contribution. The background noise removal is only important when the background noise level is close to the sampled level.

1-min accumulations are first flagged for obviously erroneous data. A 16-min Hanning filter is then applied to these data to generate smoothed 10-min accumulations. The estimated instrumental error for 10-min-

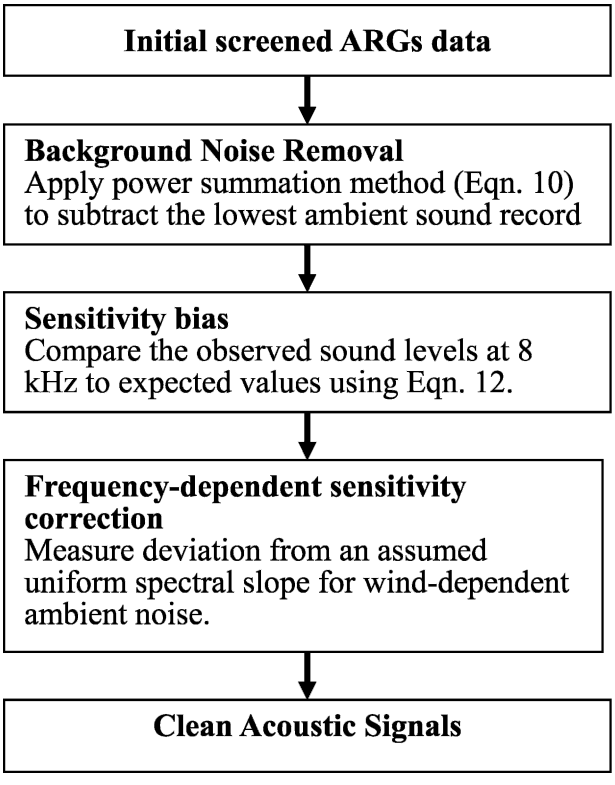

FIG. 6. The sensitivity correction flowchart.

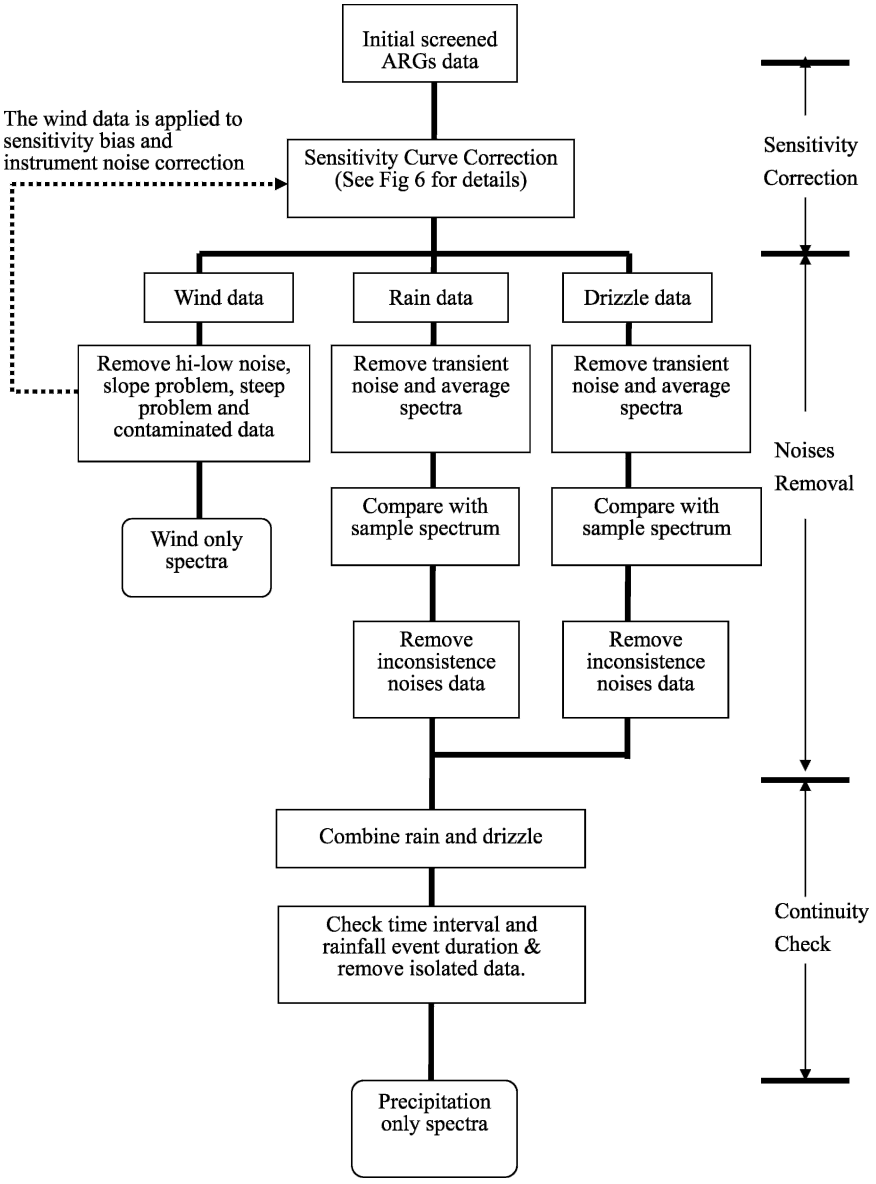

FIG. 7. Acoustic discrimination process.

derived rainfall rates is 0.4 mm h^{-1} when rain present, and is 0.1 mm h^{-1} when there is no rain (Serra et al. 2001).

b. *TRMM precipitation product 3B42*

TRMM is a satellite dedicated to the measurement of precipitation in the Tropics. The *TRMM* satellite was launched on 27 November 1997 and has maintained an altitude of approximately 350 km and an inclination of 35° to the equator. The satellite acquires approximately 16 orbits of data per day for mapping of tropical rainfall between latitudes of 38° north and south of the equator. Rainfall sensors include a precipitation radar (PR), the TRMM Microwave Imager (TMI), and a Visible and Infrared Scanner (VIRS). Data from these instruments are combined in a variety of ways to produce rainfall products that are available through the National Aeronautics and Space Administration (NASA) Goddard Distributed Active Archive Center (DAAC). Several levels of process are used in producing different products. The daily precipitation product 3B42 is produced from spatially averaged data on a 1° × 1° grid, which combines the rain structure (2B31) and VIRS calibra-

tion (1B01) to adjust IR estimates from geosynchronous IR observations. Global estimates are made by adjusting the Geostationary Operational Environmental Satellite (GOES) precipitation index (GPI) to the TRMM estimates.

5. Sensitivity correction for deep ocean geometry

a. Background noise removal—Power summation method

The ocean ambient sound–measuring sites in the ITCZ and Pacific warm pool are away from coastal regions with the depths of over 3700 m, minimizing bottom-reflection affects and biological sources associated with continental shelves. At the times when all other sources (P_r, P_w, P_{ss}, P_{ml}, P_{st}) are absent, the only source that is left will be background noise. For a given time period the background noise can be defined as minimum of the measured records $P_{bk} = \min[P_a(t)]$. Because the background noise is the smallest contributor to the overall sound pressure, removing the P_{bk} from the signal will be important only if the other sources are also small. To eliminate P_{bk} from acoustic measurement, we note that

$$P_c^2 = P_a^2 - P_{bk}^2 - 2P_aP_{bk}, \tag{7}$$

where the P_c^2 is the root-mean-square pressure without background. Because the P_{bk} is assumed to be a small independent term, the cross term P_aP_{bk} is assumed to be zero. This leads to

$$P_c^2 = P_a^2 - P_{bk}^2. \tag{8}$$

Thus, the background noise can be eliminated by the following manipulation:

$$10\log_{10}(P_c^2) = 10\log_{10}(P_a^2 - P_{bk}^2), \tag{9}$$

$$P_a^2 - P_{bk}^2 = 10^{(\mathrm{SPL}a/10)} - 10^{[\min(\mathrm{SPL}a)/10]}. \tag{10}$$

The ARGs only record the power spectrum density data in order to save onboard storage space. Equation (10) provides a means to remove the background noise from the data. The typical background level at 8.5 kHz is about 27.5 dB relative to $1\mu\mathrm{Pa}^2\ \mathrm{Hz}^{-1}$; the corresponding correction for different measured sound levels is shown in Table 3. An example of full spectral correction before and after background noise removal is shown in Fig. 5. The background noise causes only minor correction to the medium to high sound level, but is important when the SPL is similar to the background level.

Rainfall rate (mm/hr) Every 10 minutes		Decision (ARGs spectra) Rain	Decision (ARGs spectra) No-Rain
Input RMY R: Rainfall rate (mm/hr)	Rain	**Correct** Pd(R) Criteria: RMY ≥ 0.4 mm/hr; ARG detected at least one precipitation spectra.	Missed Pm(R) Criteria: RMY ≥ 0.4 mm/hr; No ARG detection at all.
	No-Rain	**False Alarm** Criteria: RMY < 0.4 mm/hr. ARG detected at least one precipitation spectrum.	**Correct** (Null decision) Criteria: RMY < 0.4mm/hr; No ARG detection at all

FIG. 8. The binary optimal decision matrix scheme. The input is the R.M. Young self-siphoning rain gauge 10-min rainfall. The output decision is the ARG precipitation detection.

b. Sensitivity bias and instrument noise

The frequency-dependent sensitivity correction is an important process that needs to be addressed before there is further data analysis, especially if the SPL will be used to quantify the geophysical signal. The hydrophone manufacturer provides a receiver sensitivity correction that is produced from a single-point source. But, in the ocean, the ambient sound source is from a broad surface area. If one applies a known uniform source in the laboratory, and then integrates the receiver sensitivity correction for multiple paths, the sensitivity correction can be acquired for the geometry of ambient sound measurement. But this is very difficult to achieve, even in an environment-controlled laboratory. The geometry of the open ocean is very different from the confined laboratory environment. Thus, a new approach is tried, which assumes that the sensitivity correction of the open ocean is the sum of the receiver-sensitivity correction, sensitivity bias, and the instrument noise. It has the following form:

$$\mathrm{SC}(f) = \mathrm{SC}_b + \mathrm{SC}_i(f), \tag{11}$$

where SC is the overall sensitivity correction, SC_b is the sensitivity bias, SC_i is the (frequency dependent) instrument noise, and the units are dB relative to $1\mu\mathrm{Pa}^2\ \mathrm{Hz}^{-1}$.

The wind-generated noise is produced by agitation of the surface water and includes bubble noise created by breaking waves and surf. Wind spectra have a constant negative slope versus logarithmic frequency with sound levels decreasing above 500 Hz at a rate of about 6 dB

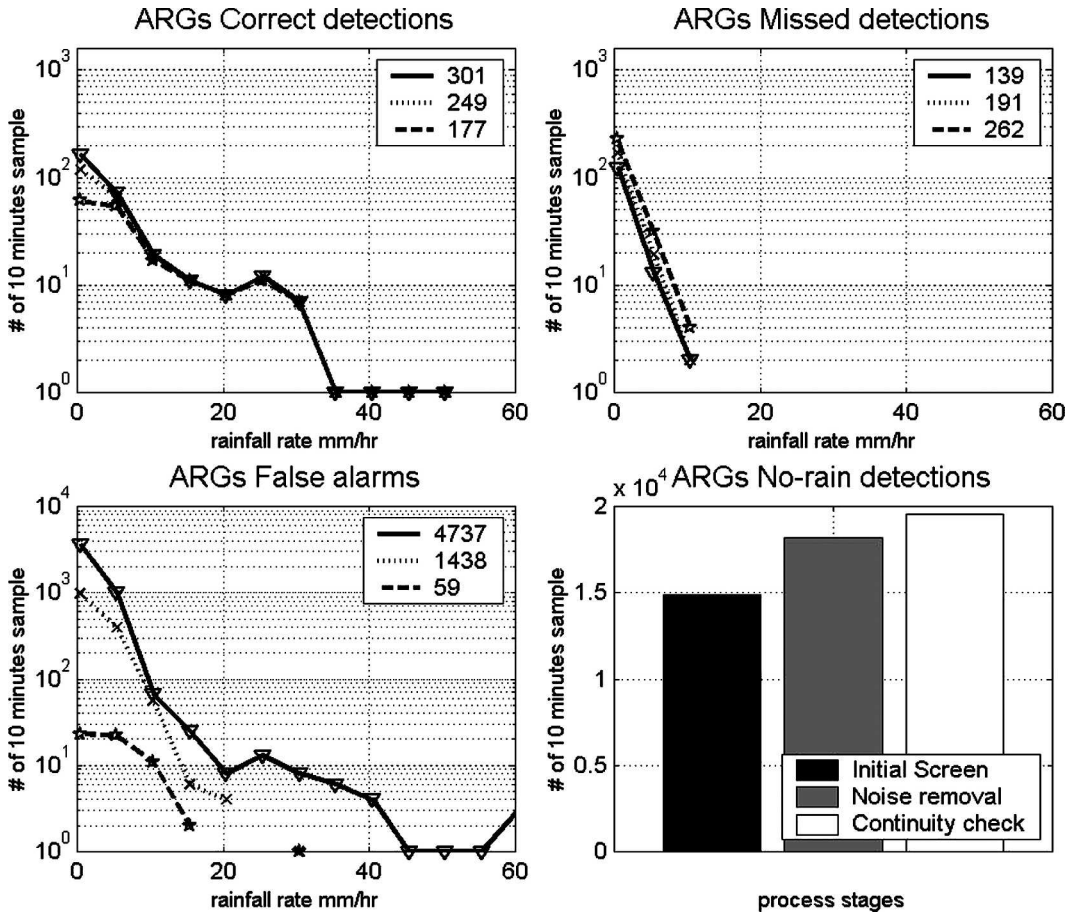

FIG. 9. Optimal decision matrix of detection in different discrimination process stages. The solid line is the initial screening using Eqs. (4) and (5). The dotted line is after noise removal, but before the continuity check, and the dashed line is the final product after the continuity check. The number in the legend boxes represents the overall number of samples in each category. The data are separated into a 5 mm h^{-1} bin width. The rainfall rate used for the correct and missed detection categories are from the R.M. Young surface rain gauge, while the rainfall rate for the false alarm category is from the of ARG data using Eq. (17).

per octave (Knudsen et al. 1948; Wenz 1962; Urick 1983). Vagle et al. (1990) proposed an algorithm between wind speed and SPL at 8 kHz, and they suggested that averages greater than at least 3 h are needed to obtain reliable wind estimates from the ambient sound

$$W = [10^{\left(\frac{\mathrm{SPL}_{8\mathrm{kHz}}}{20}\right)} + 104.5]/53.91, \qquad (12)$$

where W is wind speed at 10-m height (m s^{-1}).

The surface anemometers were collocated on all of the moorings. Thus, an expected "wind only" sound level can be predicted by applying Eq. (12). The sensitivity bias SC_b is the offset from measured SPL values at 8 kHz. The frequency-dependent instrument noise SC_i is found by assuming a uniform slope for the wind spectra and using a linear regression to find deviations. The corrected signal is given by

$$\mathrm{SPL}c(f) = \mathrm{SPL}(f) - \mathrm{SC}(f), \qquad (13)$$

where SPL$c(f)$ is the corrected acoustic signals (dB relative to 1 μPa^2 Hz^{-1}). A flow diagram for this process is shown in Fig. 6 with further details described in appendix A.

6. Acoustic discrimination process

The basic concept of the acoustic discrimination process is to use the unique spectral and temporal characteristics of different types of rainfall to detect the present of precipitation. Spectra that are not consistent with expected geophysical signals are assumed to be "noise" and are removed from the data. The acoustic data are divided into wind and precipitation (rain and drizzle) detecting according to the initial screening

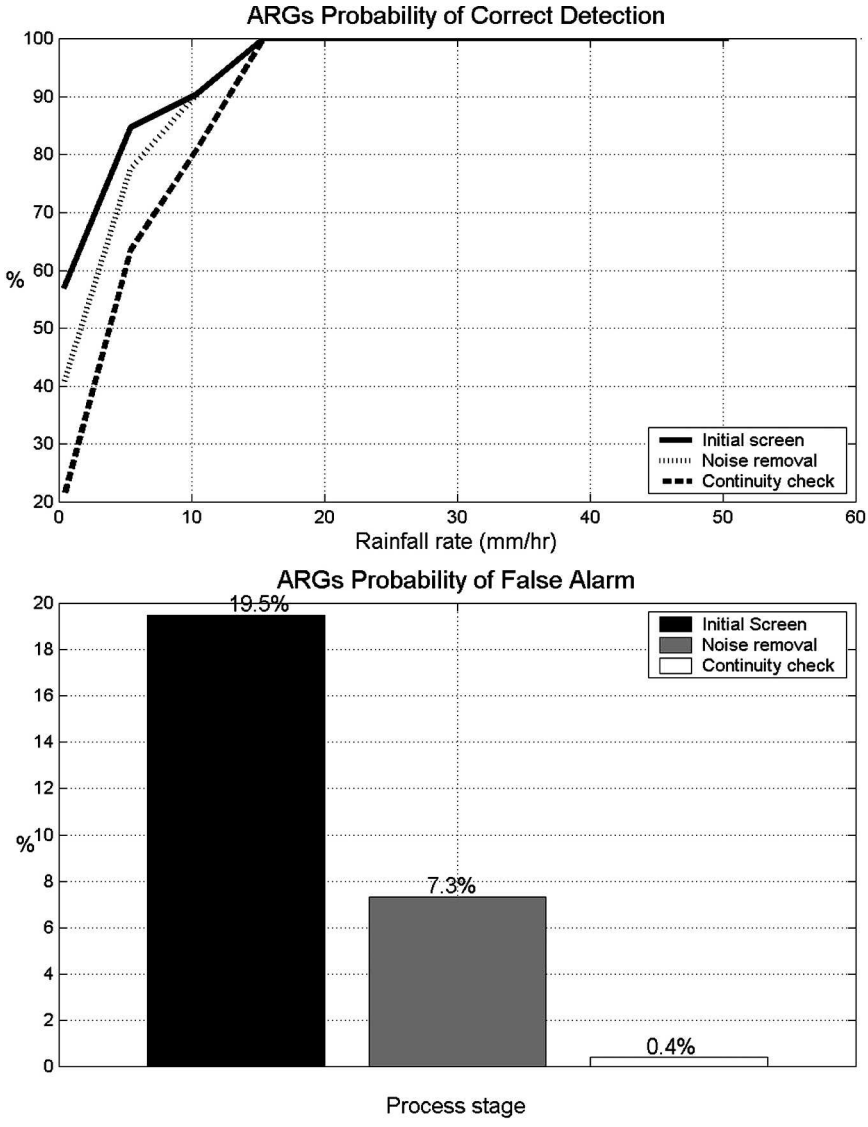

FIG. 10. The probability of correct detection is calculated from the correct and missed categories in the binary decision matrix. The probability of false alarm is calculated from the false alarm and null decision categories.

[Eqs. (4) and (5)] and are treated separately. For the wind-detection data, one spectrum was stored during the initial screening at the data collection; five different types of spectral shape tests are applied; see appendix B for details.

For data initially classified as precipitation detecting [Eqs. (4) and (5)], sets of four spectra are stored, and each are separated by 5 s. The discrimination process removes two types of noise. The first is associated with "bangs," when one of the spectra in the group of four is much louder than the other three. For example, a wave slap on the hull of the surface buoy would produce a loud noise detected by just one of the measured spectra. Assuming that the rainfall signal is continuous over at least 20 s, then such a transient noise is inconsistent with rainfall and the record is flagged as being noise. The second test is similar to the wind-detection noise test and uses the shape at the recorded spectrum to eliminate sound spectra that are not consistent with known rainfall signals. Three sample spectra that represent drizzle, light rain, and strong rain are used for comparison with observed spectra in all frequency bands. If the observed spectra are inconsistent with these sample spectra, the spectrum will be flagged and rejected. Finally, there is a continuity check. This assumes that real geophysical events (rainfall) are longer

TABLE 4. Probability of false alarm after discrimination process.

ARG	Deployment period (month)	Probability of false alarm (%)
K	5	0.4
C	5.5	0.2
D	5	0.3
B	5	0.5

than a single data point. Any isolated measurement is removed by checking the reoccurrence of rainfall signals. The sequence of the overall discrimination process is shown in Fig. 7, and details and illustrations are given in appendix B.

7. Evaluation of acoustic discrimination process in rainfall

To evaluate the success of the acoustic discrimination process, a simple optimal decision matrix, the binary decision statistic (Urick 1983) is adopted (Fig. 8). The input data are the R.M. Young surface rainfall rates for 10-min intervals, and with a "positive" detection threshold set at 0.4 mm h^{-1}. The ARG rain detection is set as the output decision. Correct detection, missed detection, and false alarm categories are further binned into rainfall rates with a bin width of 5 mm h^{-1} (Fig. 9). The following three different process stages: 1) initial screening (solid line), 2) noise removal (dotted line), and 3) continuity check (dashed line), are shown in this evaluation. Initially the false alarm rate is very high. After the discrimination process the false alarm rate became acceptable. The trade-off to this reduction in false alarm is the shift of "correct decisions" to "missed detections." However for rainfall rates higher than 15 mm h^{-1}, the discrimination process does not shift any correct decisions to missed detections, while the false alarm rate drops to nearly zero. This is illustrated again in Fig. 10. The probability of detection is calculated from the ratio of correct to missed detections. The probability of detection is increased as the rainfall rate increases, and reaches 100% when the rainfall rate is over 15 mm h^{-1}. The probability of false alarms is calculated from the ratio of the false alarm and null decision (no rain in both instruments). Through the discrimination process, the probability of a false alarm is reduced from 19.5% to 7.3% (after noise removal), to the final 0.4% (after continuity check). The discrimination process has eliminated most of the false alarms and

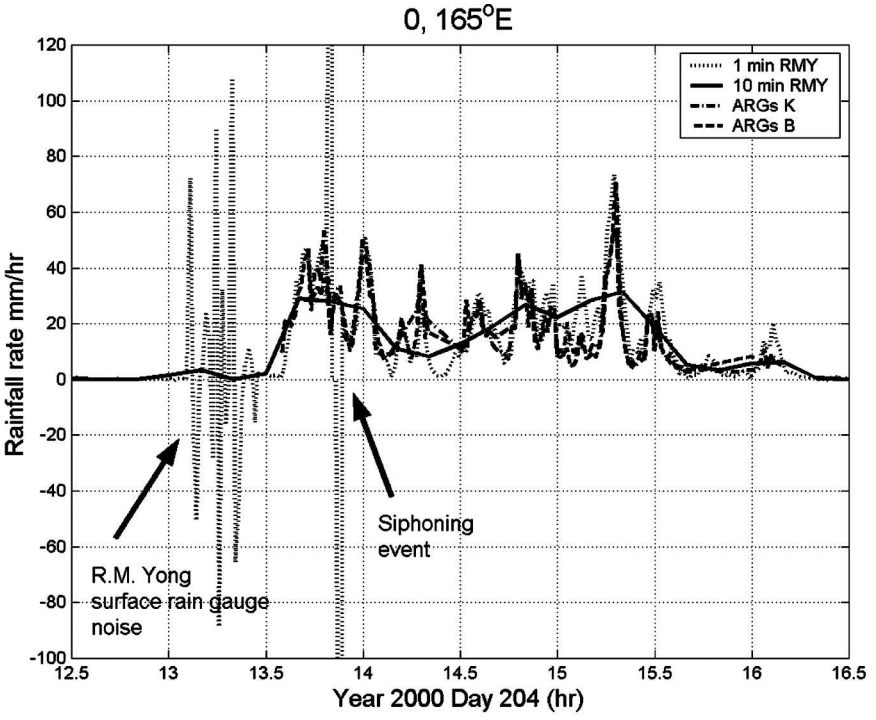

FIG. 11. The rainfall-rate comparison between the two K and B ARGs, and the 1- and 10-min R. M. Young surface rain gauge. The ARG rainfall conversion uses Eq. (17). The K and B ARGs are collocated on the same mooring at 0°, 165°E, which was deployed at the depths of 50 and 20 m, respectively.

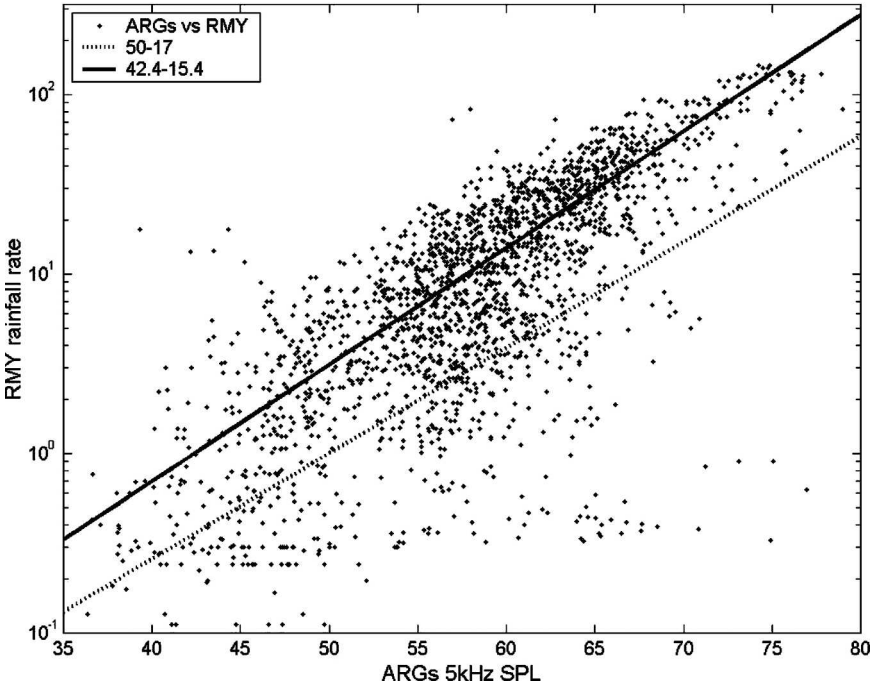

FIG. 12. Shown are 2081 min of ARG and R.M. Young 1-min sampling interval rainfall (mm h^{-1}) data that have been used in the orthogonal linear regression for SPL at 5 kHz and the logarithmic rainfall rate. The dotted line is from Nystuen (1996), and the solid line is R.M. Young 1-min vs ARG 1-min data after removing the outliers, which are defined by the last 10% of density distribution. The numbers in the legend box represent a' and b' in Eq. (15) for each regression line.

still maintained a high probability of detection, at least for a rainfall rate over 5 mm h^{-1}. The sources of errors in this analysis will be the detection errors from both instruments because the true rainfall is unknown and errors are possible for both instruments. The probability of false alarm from several ARG deployments is shown in Table 4.

8. Rainfall quantification—Empirical algorithm for deep open ocean

A simple relationship between sound intensity and rainfall rate (mm h^{-1}) can be written in the form of

$$I = aR^b, \tag{14}$$

where I is the sound intensity and R is the rainfall rate.

Taking 10 $\log_{10}$ of Eq. (14) at 5 kHz, this becomes

$$\mathrm{dB}R/10 = (SPL_{5\mathrm{kHz}} - a')/b', \tag{15}$$

where $\mathrm{dB}R = 10\log_{10}(R)$, a' represents the intercept and b' is the slope. The acoustic rainfall signal at 5 kHz is chosen because it has a large dynamic range and is in a part of the acoustic spectrum that is not thought to be affected by wind speed (Nystuen 2001). A similar empirical algorithm of rainfall-rate conversion was proposed by Nystuen (1996) based on observations from a shallow brackish pond near Miami, Florida,

$$\mathrm{dB}R/10 = (\mathrm{SPL}_{5\mathrm{kHz}} - 50)/17, \tag{16}$$

where R is the rainfall rate (mm h^{-1}). Using the R.M. Young data as a guide for rainfall rate and the acoustic sound pressure level (dB) at 5 kHz, a new empirical algorithm for rainfall rate versus sound pressure level can be produced. Nominally, the R.M. Young rainfall product is the rainfall rate (mm h^{-1}) for 10-min intervals. This product is the result of the smoothing of 1-min rainfall-rate data with a 16-point Hanning filter. From Fig. 11 it is clear that this smoothing has removed part of the dynamic range associated with heavy rainfall. To produce an acoustic algorithm that includes a large dynamic range, a subset of the original 1-min sampling interval of R.M. Young data is used after obvious errors (negative values and siphoning events) are removed (Fig. 12). Statistical outliers, defined by the last 10% of the density distribution, are also removed before the orthogonal linear regression is calculated. Part

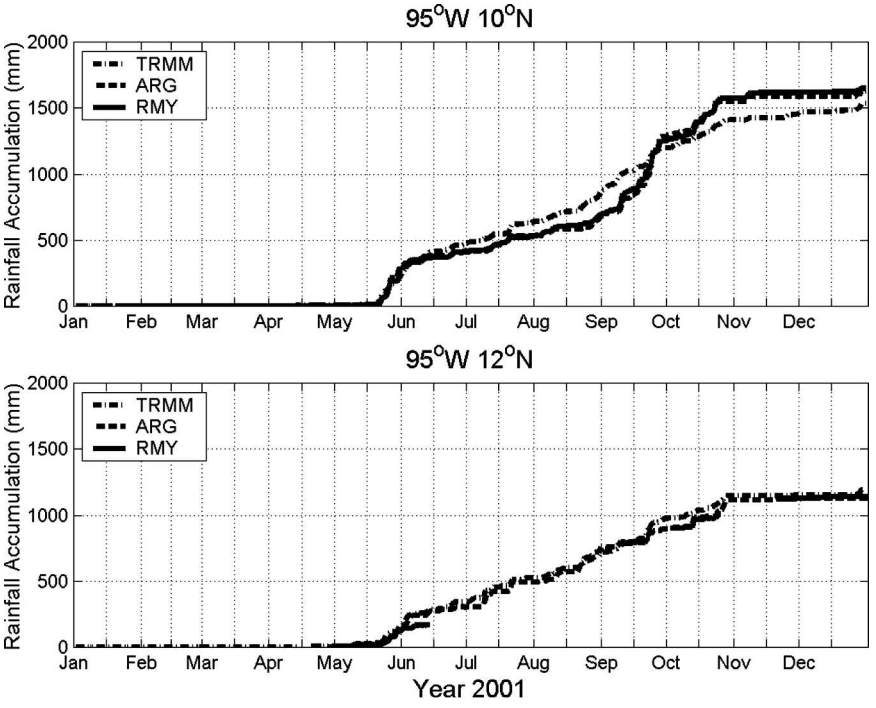

FIG. 13. The rainfall accumulation in 10° and 12°N, 95°W in 2001. The ARG (dotted line), R.M. Young (solid line), and TRMM (dashed line) rainfall accumulation (mm). (top) The ARGs and R.M. Young data have excellent agreement in both rainfall events and overall accumulation. The TRMM data also show general seasonal agreement. (bottom) The R.M. Young data were missing in some periods during the deployment. The accumulation of R.M. Young has been offset by applying the acoustic rainfall conversion data. The difference in annual rainfall estimate is less than 5%.

of the outliers, as shown in Fig. 12 with "+" signs, is thought caused by the size difference of the sampling area of these two instruments. As given in Eq. (6), the typical surface sampling area for the ARG is about 7069 m^2 when deployed at a 50-m depth. It is roughly seven orders of magnitude larger than the R.M. Young rain gauge, which has a 100 cm^2 catchment area. When a rainy cloud patch approaches from the distance, the ARG will detect the rainfall-generated sound before the R.M. Young rain gauge catches any raindrops, and similarly so when the raining cloud patch moves away. The new result suggests an algorithm for those datasets of

$$\mathrm{dB}R/10 = (\mathrm{SPL}_{5\mathrm{kHz}} - 42.4)/15.4. \qquad (17)$$

The standard deviation for the difference between the ARG estimate rainfall rate using Eq. (17) and the R.M. Young rainfall rate is in the order of 0.25. It is quite large and is most likely a result of the sampling area that is covered and the nature of the variability of rainfall. This algorithm is also quite different from the previous study. In particular, the sound level reported from the open-ocean locations appears to be nearly 10 dB quieter than those in the Miami data. Presumably, the bottom reverberation of the shallow freshwater pond versus the deep open-ocean condition is responsible for the changes in the empirical algorithm. The rainfall-rate comparison is shown in Fig. 12.

9. Validation of rainfall-rate algorithm

Rainfall accumulations for 2001 at the 10°N, 95°W and 12°N, 95°W TAO moorings are shown in Fig. 13. The acoustic rainfall accumulation is calculated by applying the rainfall-rate algorithm [Eq. (17)] and is compared with the collocated R.M. Young rain gauge and *TRMM* satellite rainfall product 3B42. This part of the ocean has a distinctive rainy season beginning in May and lasting into October. Exact agreement between the satellite estimate and the surface instruments should not be expected, because the sampling strategies are very different (spatial averaging versus high temporal resolution). However, seasonal agreement should be expected. The comparison shows that the R.M. Young

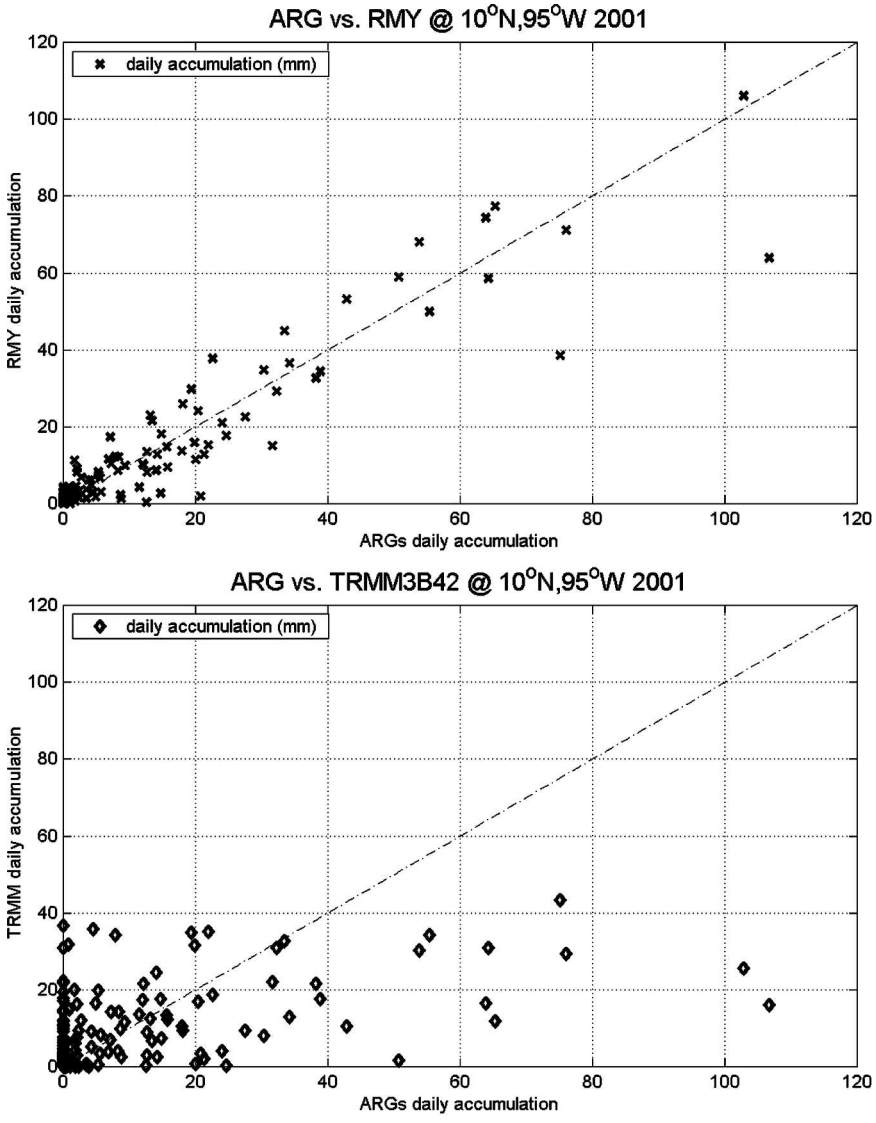

FIG. 14. The daily rainfall accumulation scatterplots. (top) The ARG vs R.M. Young rain gauge data show good agreement in daily accumulation basis. (bottom) The ARG vs TRMM product 3B42 data.

gauge and ARG at 10°N, 95°W have excellent agreement for both individual events and for the annual accumulation (Fig. 13, top). At 12°N, 95°W, the R.M. Young gauge did not function properly during several time periods (Fig. 13, bottom). The accumulation measurement of the R.M. Young data is shifted to match the ARG accumulation after each period of nonperformance. The R.M. Young and ARGs are in good agreement when both instruments were functioning properly. The ARGs also has very good seasonal agreement with TRMM. The difference in the annual rainfall estimate is less than 5%. The scatterplots for daily accumulation are shown in Fig. 14. The ARGs and R.M. Young gauge show very good agreement (Fig. 14, top), but the ARGs and TRMM (Fig. 14, bottom) show that the satellite measurement does not have any daily rainfall accumulation over 50 mm. This probably reflects the spatial sampling limitations of satellite rainfall estimation compared to the more localized acoustic measurement of rainfall.

10. Summary geophysical signals in deep open ocean

The wind and rain spectra from 30 buoy months of data in 2000 have been averaged and are presented in

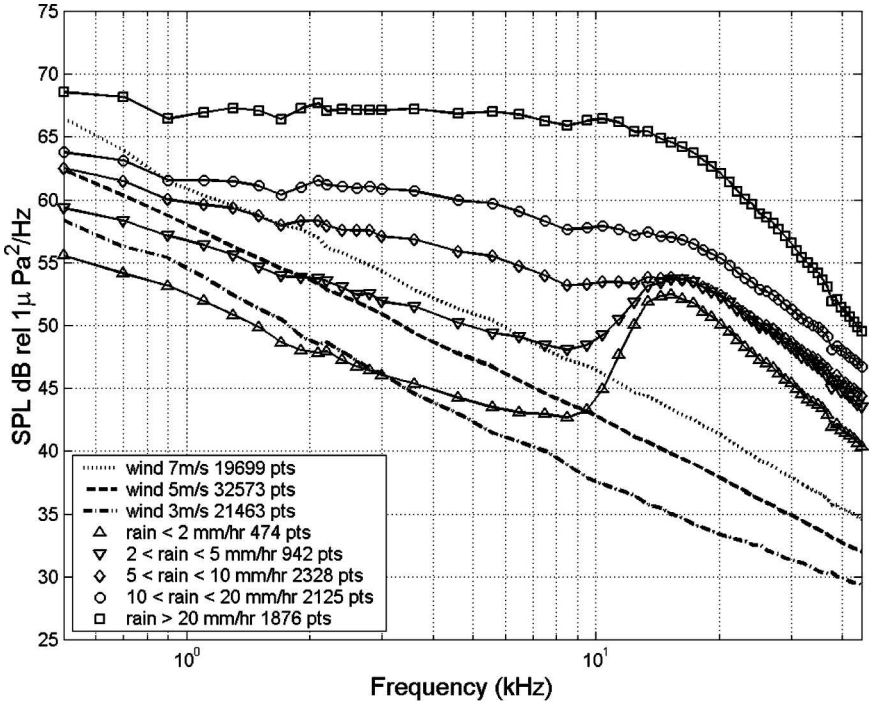

FIG. 15. The summary spectra from ARG 30–buoy months data collection. The wind-only spectra are shown with averaging wind speed at 3 (dashed–dotted line), 5 (dashed line), and 7 (dotted line) m s^{-1}, respectively. The rain spectra are averaged from each rainfall category. The numbers in the legend box indicate how many spectra have been averaged to produce the mean spectrum in each category.

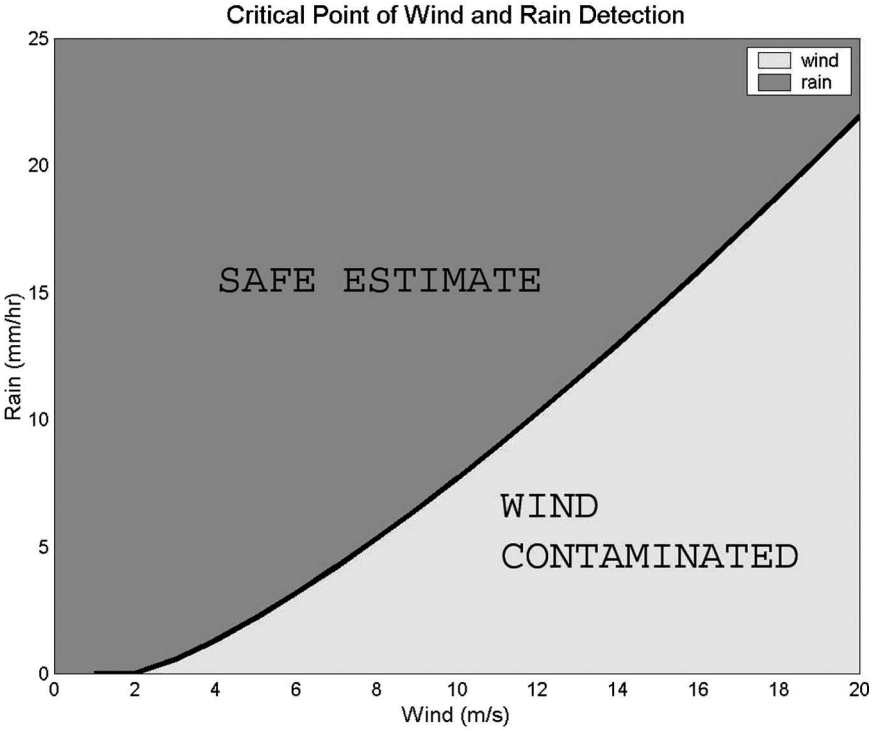

FIG. 16. This figure shows the likelihood that the measurement of the rainfall rate using Eq. (17) will be contaminated by sound resulting from wind.

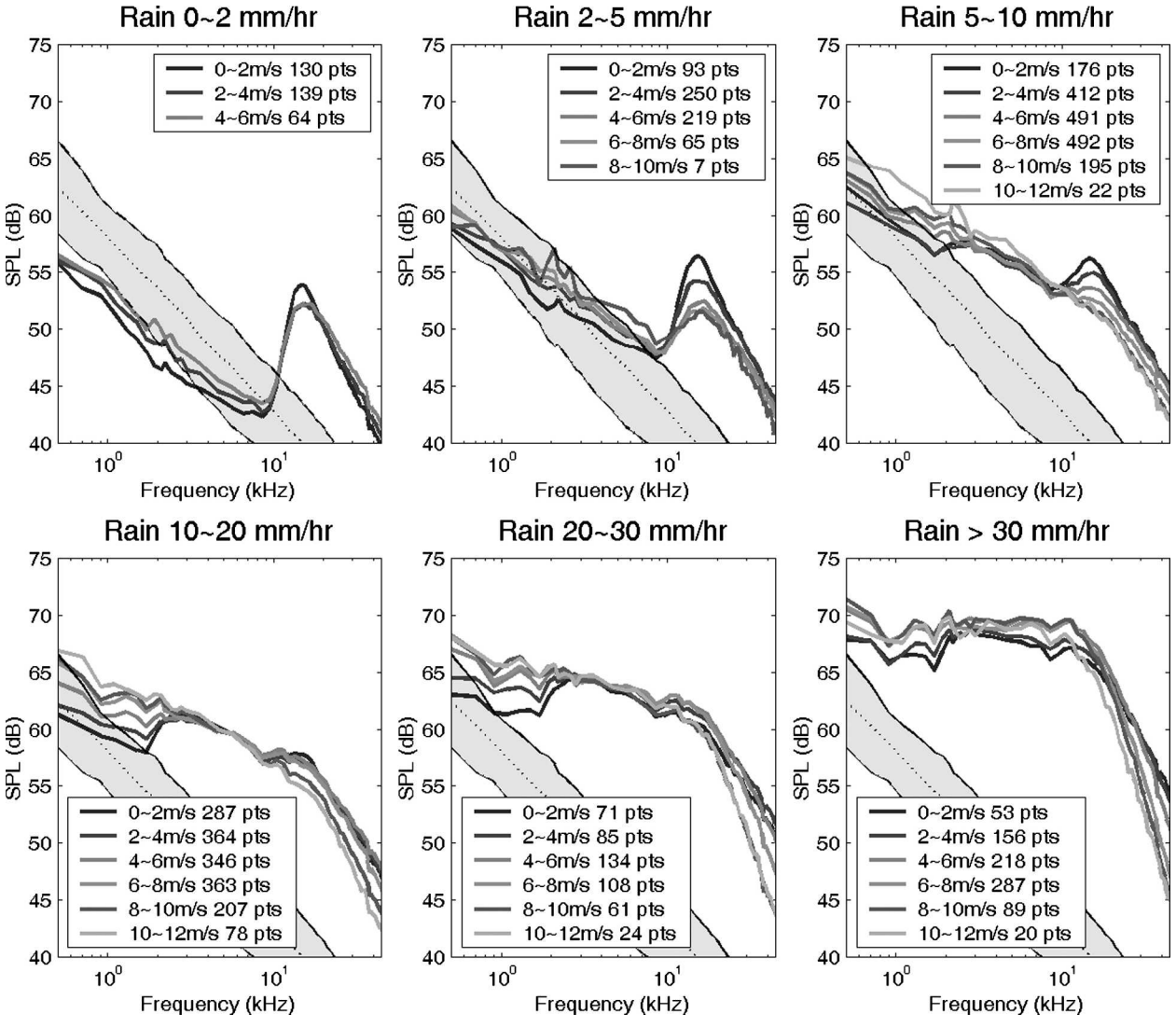

FIG. 17. The ambient sound level at a different rainfall rate vs wind speed. The data are from the L ARG at 10°N, 95°W in 2001. The numbers in the legend box indicate how many spectra have been averaged to produce each line. The gray patch is the wind-only spectrum at a wind speed from 3 to 7 m s^{-1} for reference.

Fig. 15. The wind- and rain-generated sound spectra were collected and sorted by wind speed and rainfall rate. The wind-generated spectra are shown for wind speeds at 3, 5 and 7 m s^{-1}, and the rain-generated spectra are shown for rainfall rates of <2, ~2–5, ~5–10, ~10–20, and >20 mm h^{-1}, respectively. The wind-generated sound has a distinctive sound spectrum with a constant slope of about −15.7 dB $(\text{decade})^{-1}$. The wind speed is quantified using Eq. (12). Rainfall, even light rainfall, produces loud sound levels relative to wind. For rainfall rates over 20 mm h^{-1} the signal is very loud and extends across a wide-frequency band (500–50 000 Hz). The feature in the rain spectrum at 15 kHz is a result of small raindrops within the rain (Nystuen 2001) and is not a reliable indicator of rainfall rate, but can be used to detect light rainfall.

At low frequencies, as the rainfall rate decreases, the signal is gradually replaced by wind-generated sound (from breaking waves). Or alternatively, as the wind speed increases, the sound pressure levels resulting from rainfall [Eq. (17)] will become "contaminated" by wind. Figure 16 attempts to predict when this will happen. The component of sound at 5 kHz, resulting from wind, can be predicted using Eq. (12) and adjusted to 5 kHz (+3 dB) using the observed spectral slope for wind shown in Fig. 15. Figure 16 shows the relative amplitude

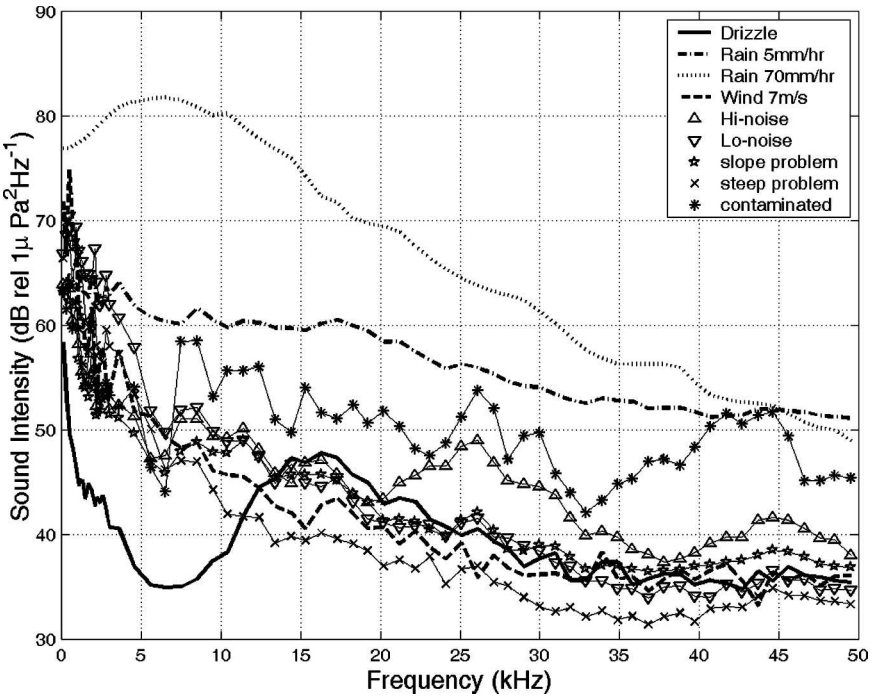

FIG. A1. The typical geophysical acoustic signals and noises. The correspondent symbols are five types of nongeophysical signals, which have been removed from sound field data.

of the sound resulting from the rainfall rate [Eq. (17)] and wind. Thus, the separation line on the plot is an indication of when the rainfall-rate algorithm is valid. This prediction assumes that rain does not affect the sound generated by wind, and that the sound produced by each process is independent, at least at 5–8 kHz. In fact, it is "known" that rain suppresses wave breaking, and so the sound present in heavy rain and high-wind conditions needs further investigation.

The rainfall spectra as a function of wind speed are further decomposed in Fig. 17. The rain signal from 2 to 10 kHz is relatively independent of wind speed, validating the choice of 5 kHz for the acoustic rainfall-rate algorithm. But, the signal at 15 kHz produced by small raindrops, which is most apparent at light rainfall rates (drizzle), is highly dependent on wind speed. This is expected because the probability that an individual small raindrop will produce a bubble decreases linearly from 100% at a normal incident to 10% for oblique incidence 20° from the vertical (Nystuen 1993). And, finally, the slope above 30 kHz in the heavier rainfall-rate categories shows the sound level decreasing as wind speed increases. This is probably not a result of a reduced sound source, but rather results from bubbles just below the surface, which mask the signal generated at the surface. These ambient bubbles would attenuate surface-generated sound and mask an acoustic measurement below the bubble layer. Potentially, this change in the shape of the spectrum can be used to measure the ambient bubbles themselves.

11. Conclusions

The rainfall measurement over the ocean using ambient sound relies on the accuracy of the sound pressure level measurement. A calibration method is demonstrated by using the expected sound signal from the wind. Using months of collocated wind speed data, the sensitivity bias and instrument noise for each ARG can be derived, providing a frequency-dependent sensitivity correction. After applying this sensitivity correction, an empirical rainfall conversion algorithm that is based on a single frequency (5 kHz) is proposed and tested on the yearlong deployment at 10°N, 95°W and 12°N, 95°W in 2001. The results show the excellent agreement in both rainfall events and the yearlong accumulation in between R.M. Young rain gauges and ARGs, and seasonal agreement in between TRMM satellite data and ARGs.

Part of the acoustic rainfall measurement is the objective detection of rain. An acoustic discrimination method based on the frequency characteristics of the observed ambient sound spectrum and temporal reoc-

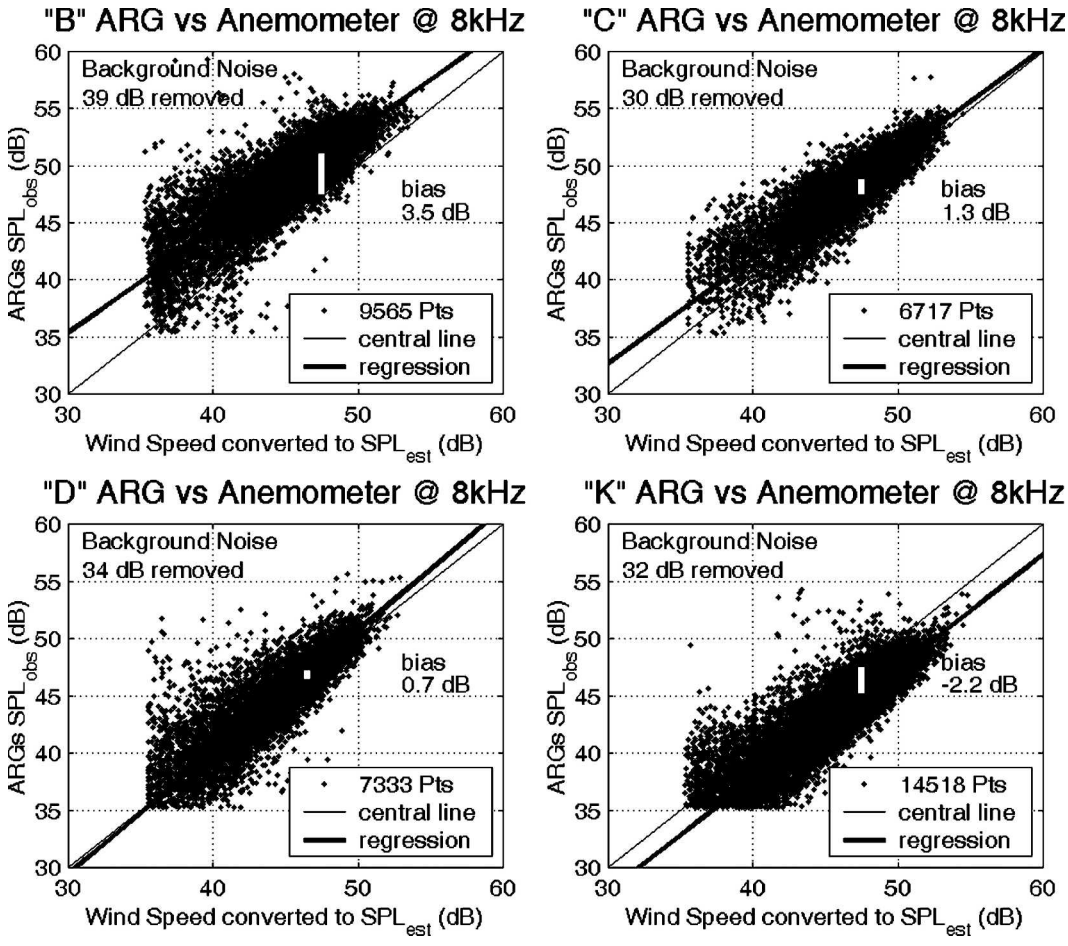

FIG. A2. The sensitivity bias corrections of different ARGs. The SPL_{est} is produced by using Eq. (12), and the SPL_{obs} is from ARG measurement at 8 kHz.

currence is successful at retrieving the rainfall acoustic signals. The probability of false alarms is reduced to 0.4% after the discrimination process. For rainfall rates over 15 mm h^{-1}, acoustic detection is nearly 100%.

The effect of wind on the acoustic signal from rain is examined and shown to be wind speed dependent. At lower frequencies, the signal from rainfall becomes "contaminated" by the sound produced from waves breaking. Contamination is frequency dependent and can be estimated. However, this separation may not be valid, especially at high rainfall rates and high wind speeds, because the interaction of rain with the sound production mechanism for wind (breaking waves) is not fully understood. The unique spectral feature of light rain—a peak in the spectrum at 15–25 kHz—is affected by wind. This spectral peak is a result of the sound generated by small raindrops within the rain and is not a reliable indication of rainfall rate, but can be used to detect rainfall, even light drizzle. Above 30 kHz, the sound levels for high rainfall rates are observed to decrease as the wind speed increases. This is likely to be a result of the attenuation of the rainfall signal by ambient bubbles that have been stirred down into the ocean and act as an absorption layer for an acoustic measurement made below the bubbles.

Acknowledgments. The ARGs in this study were deployed and collected by the Climate Research Division of PMEL NOAA, headed by Dr. Michael J. McPhaden. We wish to thank Dr. Paul Freitag, Dr. Yolande L. Serra, and Ms. Sonya Noor of PMEL, and Dr. Ren-Chieh Lien and Dr. Eric D'Asaro of APL UW for their thoughtful comments and suggestions. The satellite data used in this study were acquired as part of the Tropical Rainfall Measuring Mission. TRMM is an international project jointly sponsored by the Japan National Space Development Agency (NASDA) and the U.S. National Aeronautics and Space Administration

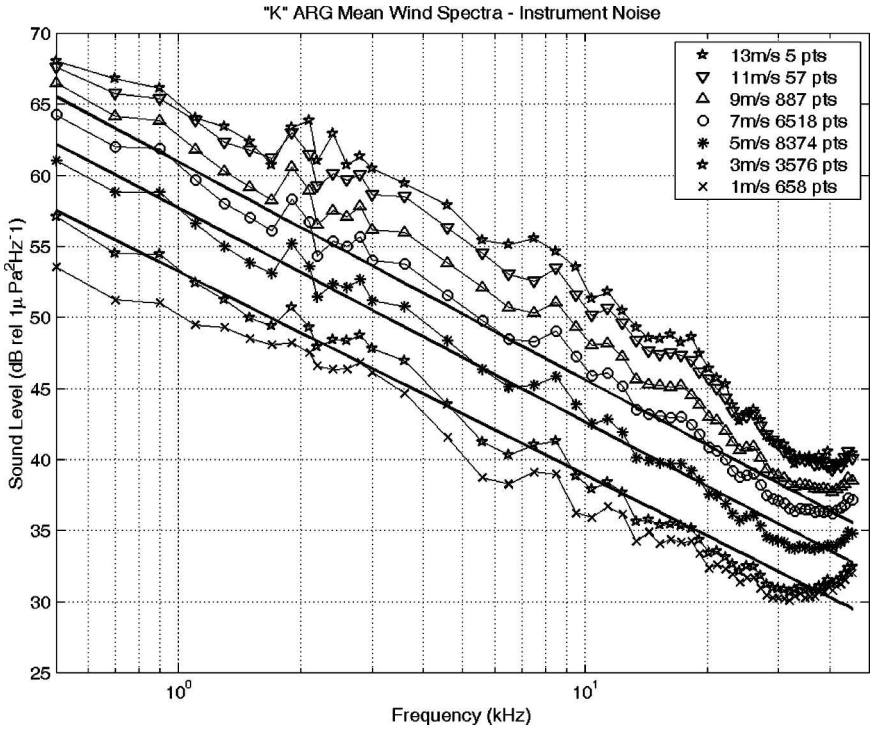

FIG. A3. Mean wind spectra in different wind speed categories. The instrument noise is acquired by applying the linear regression on the 3, 5, and 7 m s^{-1} wind speed categories and averaged the difference in between regression lines (SPL_{fit}) and observed field data (SPL_{obs}).

Office of Earth Sciences. We also wish to thank the two anonymous reviewers whose comprehensive and critical comments were vital to the revision and improvement of this manuscript. Funding is from NSF Physical Oceanography, ONR Ocean Acoustics, and the NASA TRMM Office.

APPENDIX A

Sensitivity Bias and Instrument Noises Correction

Absolute sound levels are required in order to apply geophysical conversion relationships, such as Eq. (12) and Eq. (17). And while hydrophone manufacturers provide frequency-dependent sensitivity curves, these curves are for an isolated transducer in a free field. Once the transducer is installed in an instrument, the mounting geometry of the instrument may produce a change in the sensitivity. Furthermore, the geophysical signal for rainfall or wind (breaking waves) is assumed to be a uniformly distributed planar source (the ocean surface), rather than a point source, which is typically used in laboratory calibration. Consequently, the frequency-dependent sensitivity curve is calculated post-deployment using two assumptions—first, that the wind curve of Vagle et al. (1990) is universal, and second, that the slope of the wind-generated sound spectrum is not a function of wind speed. Ultimately these assumptions will be justified by observing that the resulting rainfall-rate relation [Eq. (17)] is also universal. The steps in finding sensitivity curve follow.

a. Clean the data for nonwind noise

Data records that are initially identified as being wind are treated separately from the rain and drizzle data. The shape of each spectrum is inspected to identify noise. Five "noise" removal schemes are applied, including "low noise," "high noise," "slope problem," "steep problem," and "contaminated." Signals that are not consistent with expected geophysical signals (rain, wind, and drizzle) are called noise for the purpose of making geophysical measurements, and are as follows:

low noise: if $SPL_{2–4kHz}$ is greater than SPL_{5kHz} plus 5dB, and $SPL_{2–4kHz}$ is greater than 60 dB;
high noise: if $SPL_{15–20kHz}$ is smaller than $SPL_{20–30kHz}$, and $SPL_{15–20\ kHz}$ is greater than 35 dB;
slope problem: if $SPL_{2–4kHz}$ is smaller than SPL_{5kHZ}, SPL_{5kHz} is smaller than $SPL_{6–9kHz}$, $SPL_{6–9kHz}$ is smaller than SPL_{10kHz}, or SPL_{10kHz} is smaller than $SPL_{15–20kHz}$;
steep problem: if SPL_{5kHz} minus SPL_{10kHz} is greater than 10 dB; or

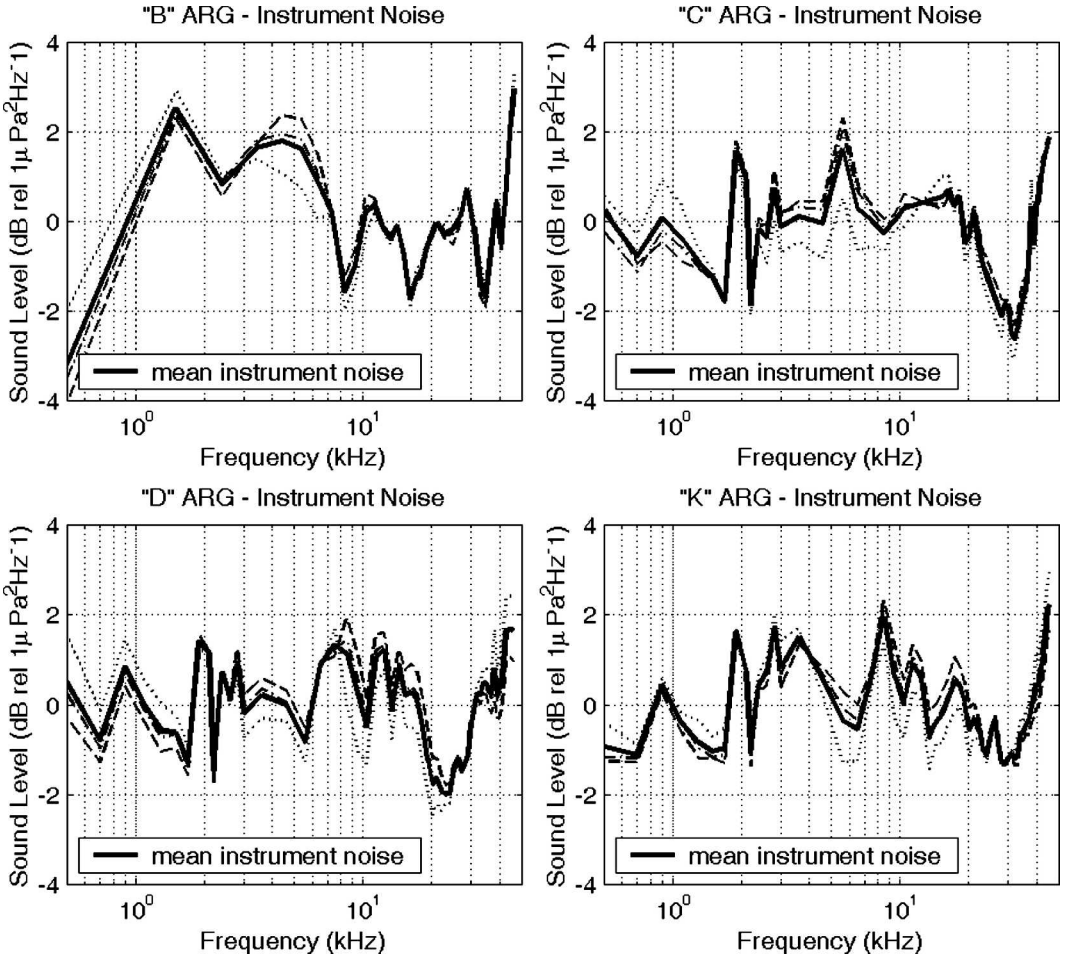

FIG. A4. The darkened lines are the mean instrument noise for each ARG, which is acquired from averaging the difference in between SPL_{obs} and SPL_{fit} of wind speeds of 2–4, 4–6, and 6–8 m s^{-1} categories.

contaminated: if SPL_{20kHz} is greater than 50 dB (not wind-only spectrum).

Figure A1 shows some individual examples of such noise. The nongeophysical signals could be produced by the noise from the mooring lines or water splashing on the buoys, or biological sources.

b. Remove low-wind data

When there is no wind-generated signal present it means that the acoustic signal recorded is a combination of electrical instrument noise and location-dependent background ocean noise. The wind speed is assumed to be less than 3 m s^{-1}.

c. Identify sensitivity bias

The anemometer data are used to find the expected sound level at 8 kHz using Eq. (12).

The mean difference is found between these sound levels and the observed sound levels (Fig. A2). This offset at 8 kHz is defined to be the sensitivity bias. The bias for ARG "B" is +3.57 dB. The data are offset by this bias.

d. Identify frequency-dependent instrument noise

The shape of the wind-generated sound spectrum is independent of wind speed for wind speeds less than about 8 m s^{-1} (Vagle et al. 1990). Above 8 m s^{-1} an attenuation by trapped bubbles changes the shape of the spectrum (Farmer and Lemon 1984) at higher frequencies, above 8 kHz. This is shown in Fig. A3. Using the anemometer wind speeds, the data have been partitioned into wind speed bins of 0–2, 2–4, 4–6, 6–8, 8–10, and over 10 m s^{-1}.

Small-scale frequency structure is present in these spectra. This is assumed to be residual frequency-

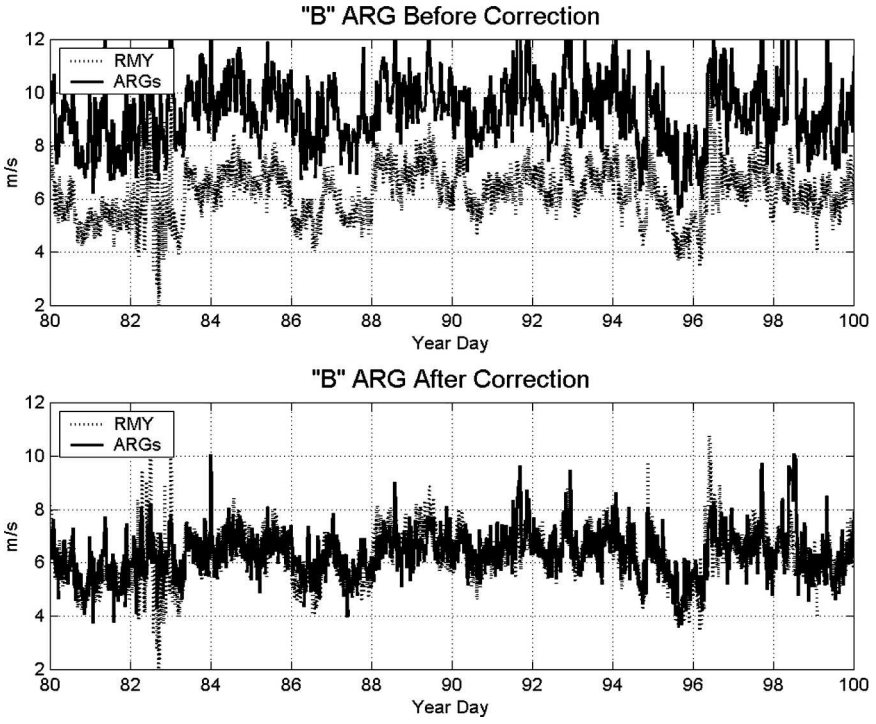

FIG. A5. The wind speed comparison in between the B ARG and R.M. Young surface anemometer: (top) the time series before the sensitivity correction, and (bottom) the time series after the sensitivity correction.

dependent instrument sensitivity. Using only the 2–4, 4–6, and 6–8 m s^{-1} bins, a linear regression is applied to the averaged spectrum in each bin (Fig. A3). These lines are parallel for 500 Hz–45 kHz, supporting the assumption that the shape of wind-generated sound spectrum is independent of wind speed for this wind speed range (2–8 m s^{-1}) (Medwin and Beaky 1989; Vagle et al. 1990). The differences between the regression lines and averaged spectra are further averaged to produce the frequency-dependent instrument noise correction for each ARG (Fig. A4). This procedure could remove a true frequency-dependent structure in the wind- generated sound spectra associated with the source mechanism (bubbles from breaking waves (Medwin and Beaky 1989). However, the source mechanism for rainfall is different [bubbles from raindrop splashes (Medwin et al. 1992; Nystuen 2001)], and should not show the same finescale frequency dependence as the wind. Mean rain-dependent spectra are shown in Fig. 15, along with mean wind speed–dependent spectra. Neither show the finescale frequency dependence of the sensitively correction, confirming that instrument noise has been removed by this procedure and not by part of the geophysical signal. The wind speed comparison before and after the sensitivity correction of the B ARG are shown in Fig. A5. The wind speed comparison does not match well before the correction, but after the correction, the agreement is excellent. The daily wind speed comparison of the ARG "C" after correction is shown in Fig. A6, which has very good agreement in both the scattering plot and time series. The correlation coefficient and standard deviation of the ARG–converted wind speed and R.M. Young anemometer are shown in Table A1.

APPENDIX B

Acoustic Discrimination Process

a. Initial sorting of the acoustic data

Objective tests on the shape of the spectrum are used to control the time step of data collection in the ARGs. This time step is used to sort the data into three categories—wind (no rain), drizzle, and rain. For the data considered here, the temporal resolution of wind-triggered data is 8–9 min, with one spectrum stored; drizzle has a 3- or 4-min interval, with four spectra stored; and rain has a 1-min interval, with four spectra stored. These data contain noise from nongeophysical sources. This noise must be identified and removed.

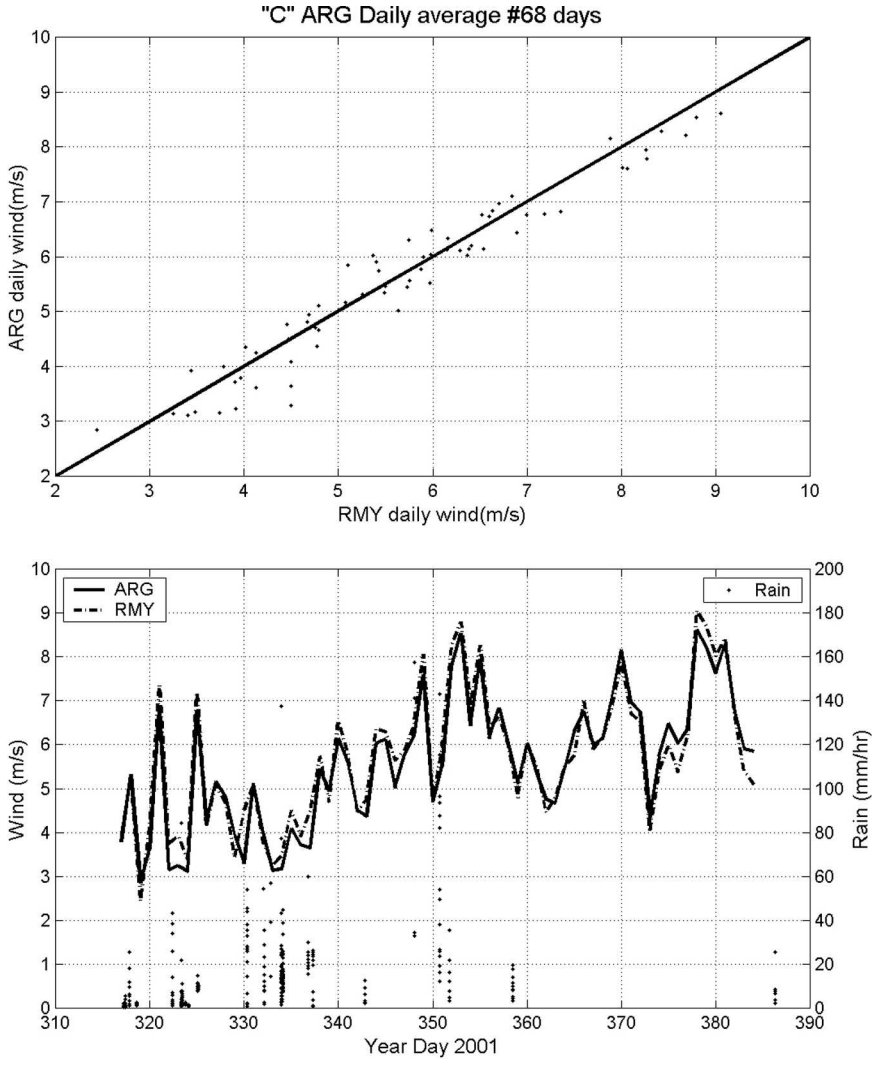

FIG. A6. The C ARG daily wind speed comparison after the sensitivity correction: (top) the scatterplot of daily wind speed for 68 days, and (bottom) the daily time series of wind speed comparison. The ARG rainfall rate is also shown with the scale on the right-hand side.

b. Remove the transient sound "bangs" and average over spectra

Data records that are initially identified as drizzle or rain can also contain nongeophysical noise. These records are actually recorded as four individual spectra, separated by 5-s intervals. An assumption is made that the geophysical signal is continuous over this 20-s period. If one of the spectra is significantly louder than the others, then a "bang" is assumed to be present. Two types of bangs are defined as follow:

$$\Delta \mathrm{SPL}_{5\mathrm{kHz}} = \max(\mathrm{SPL}_{5\mathrm{kHz}}) - \min(\mathrm{SPL}_{5\mathrm{kHz}}) > 5 \text{ dB: low-bang present;}$$

$$\Delta \mathrm{SPL}_{25\mathrm{kHz}} = \max(\mathrm{SPL}_{25\mathrm{kHz}}) - \min(\mathrm{SPL}_{25\mathrm{kHz}}) > 5 \text{ dB: high-bang present.}$$

If no bangs are present, the precipitation record is assumed to be good and is the average of the initial four spectra. If only one of the spectra has a (high or low) bang, then the precipitation record will be the average of the remaining three spectra. If more than one spectra

TABLE A1. The correlation coefficient and standard deviation of each dataset after the sensitivity correction.

ARG	K	B	C	D
Correlation coefficient	0.8953	0.8122	0.8717	0.8446
Standard deviation ($m\ s^{-1}$): ARG	1.547	1.5655	1.8899	1.5908
Standard deviation ($m\ s^{-1}$): R.M. Young	1.6979	1.6979	1.9536	1.7687

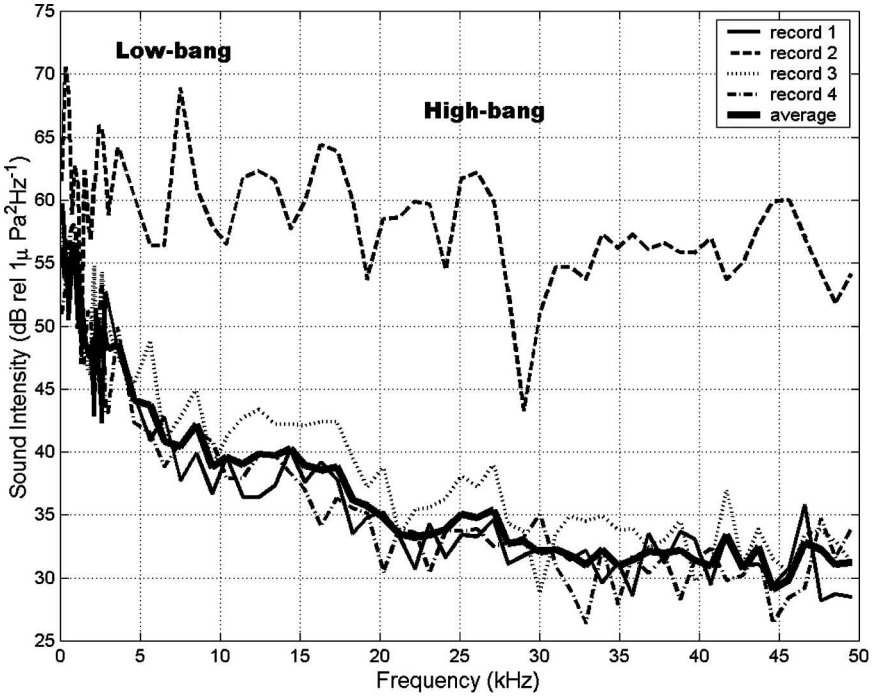

FIG. B1. The example of four spectra for precipitation-detection data. Two types of transient noises are defined as high and low bangs, and are removed from the averaging process to produce reliable 1-min sampling interval records.

has a bang present, then the record is assumed to be contaminated and is removed. The examples of high and low bangs are shown in Fig. B1. In these data, bangs appear to be associated with time periods when high currents are present at the moorings. This suggests wave slapping on the mooring hull or stress noise that is associated with the mooring line. The exact source of this type of noise is not known.

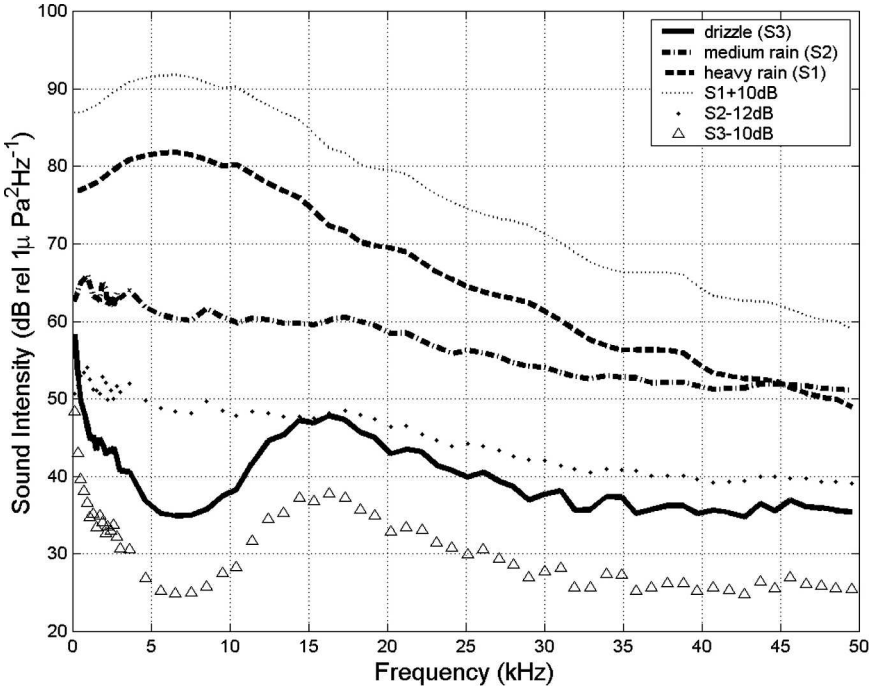

FIG. B2. The sample spectra used for identifying precipitation signals.

c. Compare with sample spectrum

Shape tests are applied to the precipitation-generated spectra to remove spectra that are not consistent with the expected signal of rainfall (Nystuen 2001). Three sample spectra—heavy (S1), medium (S2), and drizzle (S3)—are used to identify the precipitation events. The observed SPL are assumed to be in the range of S1 + 10 dB and S2 −12 dB during the rain, and in the range of S2 and S3−10 dB during the drizzle. The sample spectra are shown in Fig. B2.

d. Remove nongeophysical signals for precipitation records

Two noise removal schemes—high noise and low noise—are applied to remove the nongeophysical signals, as defined in appendix A, *a.*

e. The continuity check of rainfall event

The combination of drizzle and rain data analysis is necessary to classify the rainfall event. The continuity check is designed to remove any isolated spectrum that may have passed the noise check. The assumption is that a rainfall event must last longer than a single recording interval (1 min for rain and 3 min for drizzle). If no new rainfall signals are recorded within 10 min of a single "detection," then that detection is assumed to be false.

REFERENCES

Black, P. G., J. R. Proni, J. C. Wilkerson, and C. E. Samsury, 1997: Oceanic rainfall detection and classification in tropical and subtropical mesoscale convective systems using underwater acoustic methods. *Mon. Wea. Rev.,* **125,** 2014–2024.

Fairall, C. W., E. F. Bradley, D. P. Rogers, J. B. Edson, and G. S. Young, 1996: Bulk parameterization of air-sea fluxes for Tropical Ocean-Global Atmosphere Coupled-Ocean Atmosphere Response Experiment. *J. Geophys. Res.,* **101,** 3747–3764.

Farmer, D. M., and D. D. Lemon, 1984: The influence of bubbles on ambient noise in the ocean at high wind speeds. *J. Phys. Oceanogr.,* **14,** 1762–1778.

Freitag, H. P., M. O'Haleck, G. C. Thomas, and M. J. McPhaden, 2001: Calibration procedures and instrumental accuracies for ATLAS wind measurements. NOAA/Pacific Marine Environmental Laboratory Tech. Memo. OAR PMEL-119, 20 pp.

Knudsen, V. O., R. S. Alford, and J. W. Emling, 1948: Underwater ambient noise. *J. Mar. Res.,* **7,** 410–429.

McPhaden, M. J., and Coauthors, 1998: The Tropical Ocean-Global Atmosphere (TOGA) observing system: A decade of progress. *J. Geophys. Res.,* **103,** 14 169–14 240.

Medwin, H., and M. Beaky, 1989: Bubble sources of the Knudsen sea noise spectrum. *J. Acoust. Soc. Amer.,* **83,** 1124–1130.

——, J. A. Nystuen, P. W. Jacobus, L. H. Ostwald, and D. E. Synder, 1992: The anatomy of underwater rain noise. *J. Acoust. Soc. Amer.,* **92,** 1613–1623.

Milburn, H. B., P. D. McLain, and C. Meinig, 1996: ATLAS buoy—Reengineered for the next decade. *Proc. IEEE Oceans'96*, Fort Lauderdale, FL, Institute of Electrical and Electronics Engineers, 698–702.

Nystuen, J. A., 1993: An explanation of the sound generated by light rain in the presence of wind. *Natural Physical Sources of Underwater Sound*, B. R. Kerman, Ed., Kluwer Academic, 659–668.

——, 1996: Acoustic rainfall analysis: Rainfall drop size distribution using the underwater sound field. *J. Atmos. Oceanic Technol.,* **13,** 74–84.

——, 2001: Listening to raindrops from underwater: An acoustic disdrometer. *J. Atmos. Oceanic Technol.,* **18,** 1640–1657.

——, M. J. McPhaden, and H. P. Freitag, 2000: Surface measurements of precipitation from an ocean mooring: The acoustic log from the South China Sea. *J. Appl. Meteor.,* **39,** 2182–2197.

Pumphrey, H. C., L. A. Crum, and L. Bjorno, 1989: Underwater sound produced by individual drop impacts and rainfall. *J. Acoust. Soc. Amer.,* **85,** 1518–1526.

Serra, Y., P. A. Hearn, H. P. Freitag, and M. J. McPhaden, 2001: ATLAS self-siphoning rain gauge error estimates. *J. Atmos. Oceanic Technol.,* **18,** 1989–2002.

Urick, R. J., 1983: *Principles of Underwater Sound.* 3d ed. McGraw-Hill, 423 pp.

Vagle, S., W. G. Large, and D. M. Farmer, 1990: An evaluation of the WOTAN technique for inferring oceanic wind from underwater sound. *J. Atmos. Oceanic Technol.,* **7,** 576–595.

Wenz, G. M., 1962: Acoustic ambient noise in the ocean: Spectra and sources. *J. Acoust. Soc. Amer.,* **34,** 1936–1956.